JAERI-M
94-021

FUSION-NEUTRON DIAGNOSTIC ON THE MICROWAVE TOKAMAK EXPERIMENT

February 1994

Toshihide OGAWA, Kazumi OASA
Katsumichi HOSHINO, Kazuo ODAJIMA
and Hikosuke MAEDA

日本原子力研究所
Japan Atomic Energy Research Institute

JAERI-Mレポートは，日本原子力研究所が不定期に公刊している研究報告書です。
入手の問合わせは，日本原子力研究所技術情報部情報資料課（〒319-11 茨城県那珂郡東海村）あて，お申しこみください。なお，このほかに財団法人原子力弘済会資料センター（〒319-11 茨城県那珂郡東海村日本原子力研究所内）で複写による実費領布をおこなっております。

JAERI-M reports are issued irregularly.
Inquiries about availability of the reports should be addressed to Information Division Department of Technical Information, Japan Atomic Energy Research Institute, Tokaimura, Naka-gun, Ibaraki-ken 319-11, Japan.

編集兼発行　日本原子力研究所
印　　刷　ニッセイエブロ株式会社

JAERI-M 94-021

Fusion-neutron Diagnostic on the Microwave Tokamak Experiment

Toshihide OGAWA, Kazumi OASA, Katsumichi HOSHINO
Kazuo ODAJIMA and Hikosuke MAEDA

Department of Fusion Plasma Research
Naka Fusion Research Establishment
Japan Atomic Energy Research Institute
Naka-machi, Naka-gun, Ibaraki-ken

(Received January 25, 1994)

A neutron diagnostic system, which was designed and constructed for the Microwave Tokamak Experiment (MTX) at the Lawrence Livermore National Laboratory, has been installed and operated on that experiment. The system consisted of two different types of neutron detectors. A plastic scintillator with a nanosecond response was used for high-speed neutron measurements for the purpose of studying the intense FEL microwave absorption process. The temporal resolution of this system was limited to 2kHz by counting statistics for standard ohmic plasma. A proportional counter array with a polyethylene neutron moderator was used to determine global neutron production for a wide range of source strengths above 10^8 n/s. This system was calibrated with a ^{252}Cf neutron source in the MTX vacuum vessel. The time behavior of ion temperature was evaluated from the neutron production rates using line-averaged electron densities for each MTX shot.

Keywords: Microwave Tokamak Experiment, Tokamak Plasma, Neutron Diagnostic, Free Electron Laser, Neutron Production Rate, Proportional Counter, Fission Counter, Plastic Scintillator, Neutron Moderator

JAERI-M 94-021

Microwave Tokamak Experimentにおける中性子計測

日本原子力研究所那珂研究所炉心プラズマ研究部
小川　俊英・大麻　和美・星野　克道
小田島和男・前田　彦祐

（1994年1月25日受理）

ローレンス・リバモア研究所で行われた「ＦＥＬマイクロ波によるトカマク・プラズマ加熱実験（Microwave Tokamak Experiment）」において、ＭＴＸプラズマの中性子測定を行った。この測定には、ＭＴＸ特有の実験条件に対応できるように、特性の異なる２種類の中性子検出器を用いた。ＦＥＬマイクロ波の吸収過程の観測を目的として、数ナノ秒の時間応答性を持つプラスチック・シンチレータを使用した。この測定系は、ＭＴＸジュール加熱プラズマに対しては、信号量と検出感度による統計誤差によって時間特性が決り、２kHzまでのサンプリング周波数で有効な測定が行えた。また全中性子発生率測定のために、中性子計数管とポリエチレン製中性子減速材を用いたダイナミックレンジの広い測定系を準備した。^{252}Cf中性子線源を用いて較正実験を行い、この測定系で1×10^{8}n/s以上の中性子発生率に対応できることがわかった。この全中性子発生率と電子密度測定から、ＭＴＸプラズマのイオン温度測定を行った。

那珂研究所：〒311-01　茨城県那珂郡那珂町大字向山801-1

Contents

目　　次

1. Introduction

1.1 Microwave Tokamak Experiment

The Microwave Tokamak Experiment (MTX) was proposed[1] in 1986 to investigate Electron Cyclotron Resonance Heating (ECRH) with intense microwaves generated by a free-electron laser (FEL) at the Lawrence Livermore National Laboratory (LLNL). It is reported that there are several advantages when applying FEL microwaves for ECRH[2]. Nonlinear effects are predicted during the absorption of GW-level microwave power[3]. Japan Atomic Energy Research Institute (JAERI) contributed to MTX under Annex VI to the Japan-US Implementing Arrangement on Fusion. JAERI supplied several types of equipment, primarily plasma and microwave diagnostics, for use on MTX. The neutron diagnostic reported in this paper was one of these diagnostics.

The basic components of MTX are shown in Fig. 1 and are the microwave source (FEL or gyrotron), a quasi-optical microwave transport system[4], the MTX tokamak, and microwave and plasma diagnostics. The typical parameters of the MTX tokamak and the FEL are given in Table 1. The MTX tokamak, which had been the Alcator C tokamak at the Massachusetts Institute of Technology (MIT), was a high-density and high-field compact tokamak device with major radius R=0.64 m and minor radius a=0.165 m. The tokamak device, power units and control system were moved from MIT to LLNL, where the equipment was operated from 1988 until the conclusion of the experiment in July, 1992. The Alcator C was designed for a toroidal magnetic field of 14 T and was operated up to 13 T at MIT[5]. The MTX operated typically at B_t=5 T, corresponding to the electron cyclotron frequency of 140 GHz. The short FEL pulses made high-speed measurements important for studying the microwave-absorption process. Several diagnostics were prepared to observe the electron response to the FEL pulses[6].

The FEL, based on the ETA-II accelerator and the ELF-II wiggler, was brought into operation by the LLNL Electron Beam Group and was limited to peak powers of 100~150 MW single pulses by poor electron beam quality in the first experimental run in 1989. Following an upgrade of the ETA-II and the IMP wiggler[7] by the MTX group, a second experimental run was made lasting from December, 1991 through October, 1992. The FEL generated microwaves at 140 GHz in intense pulses with power up to 2 GW and pulse duration of 20~30 ns using as an oscillator an approximately 10 kW microwave beam from a gyrotron.

The FEL was also operated in burst mode, with more than 30 pulses generated in a 2 kHz burst[8]. The burst mode pulses were not injected into the MTX tokamak.

Two series of ECH experiments using the FEL were conducted in MTX. In initial experiments, approximately 100 MW microwaves were transmitted to the tokamak in November, 1989. The measurements of the microwave absorption by the plasma were consistent with linear theory as expected[9]. A second series of experiments was conducted using modified ETA-II, IMP and the gyrotron in June and July, 1992[10]. Pulses injected into the tokamak at power up to 1.5 GW were used in this series, which found absorption reduced below the linear theory and in good agreement with the nonlinear predictions[11].

1.2 Neutron Diagnostic

Thermonuclear fusion of deuterium is the process of interest here. The reaction $D(D,n)^3He$ produces a neutron with an energy of 2.45 MeV. The reaction rate is a very strong function of the ion temperature. Therefore neutron measurements have been used to diagnose the ion temperature of deuterium plasmas. We were also interested in the ion behavior in ECH experiments using intense FEL-produced microwaves. High-speed measurements were important to study the intense microwave absorption process. Wide dynamic range of neutron detection was required for total neutron rate measurement to evaluate the ion temperature. We designed and constructed a neutron diagnostic for MTX in 1988 combining two different types of measurement systems, because there is no detector with the ability to provide both high-speed measurements and ion temperature measurements[12]. Table 2 gives characteristics of these measurements. One is a conventional neutron production rate measurement system using proportional counters and fission counters to estimate the ion temperatures with moderate time resolution. The other is a high-speed neutron measurement system using a plastic scintillator. This diagnostic system was shipped to LLNL and installed in the MTX tokamak in the spring of 1989. Signal cables and powered cables between detectors and electronics rack were connected in July, 1989, and we had the first neutron measurements of the MTX plasma on July 25, 1989. Then we found that the electromagnetic noise could not be neglected and that cable reworking was needed to obtain clear neutron data. After revising the cable shielding and grounding in January, 1990, the neutron system was ready for measurements of the MTX plasma. In the initial deuterium plasma operation in September, 1989, the discharges were disrupted so often that

we gave up deuterium plasma operations until the first FEL experiments were over in November, 1989. That was the reason for the neutron diagnostics getting a low priority and the noise hunting jobs being late. Stable deuterium plasma discharges became possible in April, 1990 and we began neutron measurements in MTX[13].

2. Neutron production rate measurements

Neutron production rate measurement systems must have a wide dynamic range for neutron flux detection. Our diagnostic measured the flux of neutrons without any energy discrimination using a polyethylene moderator which thermalizes fast neutrons to get high detection sensitivity. The assembly was designed to be capable of detecting neutron flux over a range of five orders of magnitude in pulse count mode.

2.1 Measurement system

Five commercial neutron detectors of varying sensitivity made by Reuter-Stokes were used in order to cover the entire range of neutron source strength with good counting statistics. The detectors are listed in Table 3 starting with the most sensitive. The detector system consisted of two ^{3}He proportional counters, a BF_3 proportional counter, and two ^{235}U fission counters. A set of these detectors was installed in the center of a neutron moderator illustrated in Fig. 2. The 1 mm layer of cadmium strongly absorbs slow neutrons. Higher energy neutrons surviving the cadmium layer pass into a 10 cm layer of polyethylene on the way to the detectors. In this layer fast neutrons are converted into thermal neutrons. The 5 cm of lead reduces any hard x-ray noise effect on the neutron signal.

Two detector assemblies in neutron moderators were placed beside MTX side ports (114 cm from the plasma axis and 86 cm below the plasma midplane). Figures 3 and 4 show the location of these neutron detectors around the MTX device. One detector assembly was in front of port B and the other was in front of port F. There were two fixed limiters inside the MTX vacuum vessel located at port B and port E. Since one detector assembly (port B) was close to a limiter and one detector assembly (port F) was not, the photoneutron rate emitted from the limiters could be estimated from the difference between the counting rate of these

we gave up deuterium plasma operations until the first FEL experiments were over in November, 1989. That was the reason for the neutron diagnostics getting a low priority and the noise hunting jobs being late. Stable deuterium plasma discharges became possible in April, 1990 and we began neutron measurements in MTX[13].

2. Neutron production rate measurements

Neutron production rate measurement systems must have a wide dynamic range for neutron flux detection. Our diagnostic measured the flux of neutrons without any energy discrimination using a polyethylene moderator which thermalizes fast neutrons to get high detection sensitivity. The assembly was designed to be capable of detecting neutron flux over a range of five orders of magnitude in pulse count mode.

2.1 Measurement system

Five commercial neutron detectors of varying sensitivity made by Reuter-Stokes were used in order to cover the entire range of neutron source strength with good counting statistics. The detectors are listed in Table 3 starting with the most sensitive. The detector system consisted of two ^{3}He proportional counters, a BF_3 proportional counter, and two ^{235}U fission counters. A set of these detectors was installed in the center of a neutron moderator illustrated in Fig. 2. The 1 mm layer of cadmium strongly absorbs slow neutrons. Higher energy neutrons surviving the cadmium layer pass into a 10 cm layer of polyethylene on the way to the detectors. In this layer fast neutrons are converted into thermal neutrons. The 5 cm of lead reduces any hard x-ray noise effect on the neutron signal.

Two detector assemblies in neutron moderators were placed beside MTX side ports (114 cm from the plasma axis and 86 cm below the plasma midplane). Figures 3 and 4 show the location of these neutron detectors around the MTX device. One detector assembly was in front of port B and the other was in front of port F. There were two fixed limiters inside the MTX vacuum vessel located at port B and port E. Since one detector assembly (port B) was close to a limiter and one detector assembly (port F) was not, the photoneutron rate emitted from the limiters could be estimated from the difference between the counting rate of these

two detector assemblies.

An electronic circuit for one detector assembly is illustrated in Fig. 5. The electronics were selected based on the requirement of high speed and high count rates capability. Table 4 gives the parameters of the electronics used in the MTX plasma measurements. The TENNELEC TC170 and TC171 are fast-risetime charge-sensitive preamplifiers which have two different types signal outputs. One is for energy discrimination measurements and the other is for timing measurements. The timing output is differentiated with a 100 ns time constant. The output polarity is the same as the input polarity, which is negative voltage for our neutron counters. The TC170 is intended for use with detectors having an equivalent capacitance from 0 pF to 100 pF and the TC171 was for 100 pF or more. We used TC170 for the ^{3}He counters and BF_3 counters and TC171 for the ^{235}U counters. The timing output was selected in our measurements. Three types of high voltage power supplies were used for neutron-detector bias, depending on the required voltage. The TENNELEC TC952 is a high voltage power supply which provides 3 kV output at currents up to 10 mA. The TENNELEC TC953 is a dual high voltage supply which offers two independent outputs up to 1 kV at currents of 100 μA. The ORTEC 478 high voltage power supply provides 2 kV at 1 mA. The ORTEC 579 is a fast filter amplifier with 5 ns rise time and maximum 250× gain. The LeCroy 4608C is a eight channel high speed discriminator which has 150 MHz count rate capability. The threshold level is variable from -15 mV to -1 V. The discriminator has three negative outputs per channels, which supply -800 mV pulses into 50 Ω loads and have 3.5 ns to 100 ns pulse width. The TOYO T8590 is a CAMAC scaler which has eight channel inputs. Double scalers for each detector output signal were used for different sampling rate measurements. Scaler data were transported to a HP 360CH workstation, located in the MTX control room, through fiber optics using the LeCroy 8901A GPIB interface. The HP 360CH was used for neutron data acquisition and analysis. We could analyze the neutron data between each plasma shot using the stored data in the VAX computer and the computer network[14], shown in Fig. 6. Figure 7 and 8 show examples of the HP 360CH computer output for the neutron diagnostic. We usually monitored the two most sensitive channels in each of the two detector arrays (A-1, A-2, B-1 and B-2), shown in Fig. 7. Figure 8 shows the time trace of the ion temperature and the neutron production rates, discussed in following sections.

The neutron detectors and the electronics were tested with a ^{252}Cf neutron

source (S/N 401249) in May, 1989. The calibrated source strength was 81 μCi on September 8, 1987. Figure 9 shows the electronic circuits used in this detector calibration. The ORTEC 974 counter was used for counting the pulse signal instead of the CAMAC scaler because of easy handling of the data acquisition. Figure 10 shows how the neutron count rate varied with the threshold level of the discriminator. The noise rate became large below V_{TH}=-250 mV in the ^{3}He and BF_3 counters and V_{TH}=-350 mV in the ^{235}U counter. We started the first neutron measurements of the MTX plasma at V_{TH}=-500 mV. After the cable shielding was reworked and tested on real plasmas, we decided to use V_{TH}=-800 mV for the ^{3}He and BF_3 counters and V_{TH}=-400 mV for the ^{235}U counters.

The cable shielding and grounding configuration was important for eliminating electric noises from equipment around the MTX tokamak such as the liquid nitrogen pump and the bellows heater. The detector enclosure, which was a neutron moderator, was isolated from the support stand by insulated plates. Detectors and preamplifiers in the moderator were also isolated from the enclosure with wrapped kapton sheet. All cables between the enclosure and the diagnostic rack were covered with shielding tubes which connected the enclosure to the rack ground. Figure 11 shows the status of the grounding configuration. These connections made the detector enclosure and the rack appear as a single RF shield with a common ground connection. With this cable shielding and grounding work, the electro-magnetic noise could almost be eliminated except that which was synchronized to the discharge cleaning pulses. Fortunately, we could accept this noise problem because the discharge cleaning was turned off during the physics run.

Figure 12 shows the time evolution of MTX plasma parameters for shot No. 8922 on June 7, 1990. The plasma current was around 0.3 MA and the line-averaged electron density was around 2×10^{20} m^{-3}. The time evolution of neutron counts on the same shot is shown in Fig. 13. The most sensitive detector A-1 (^{3}He counter, P4-1609) was saturated at high source strengths during 0.20~0.38 s. The second sensitive detector A-2 (^{3}He counter, P4-0809) was unsaturated and had good statistics even in the region of high neutron rates. This detector worked effectively at this peak neutron level. The less sensitive detectors A-3 (BF_3 counter, P1-0809) and A-4 (^{235}U counter, P6-1608) are more useful at higher temperatures and greater neutron rate plasmas. We decided to evaluate neutron production rates and ion temperatures in standard ohmic discharges using the A-1 and A-2 detector signals.

Figure 14 shows the comparison of the neutron count rates measured at the two different toroidal locations with detectors of the same sensitivity (A-2 and B-2), for the typical ohmic plasma at B_t=6.5 T and B_t=8 T. The B-2 detector was placed by a limiter port and the A-2 detector was beside a nonlimiter port. This figure shows the same count rates for the A-2 and B-2 detector signals. It signifies toroidal symmetry of the neutron count rate in standard ohmic plasma discharges (the electron density n_e>1×10^{20} m^{-3}). We can say that photoneutrons were negligible compared with the thermonuclear fusion neutrons in ohmic plasmas of this density.

2.2 Calibration

The neutron detectors were calibrated with a ^{252}Cf neutron source (S/N 401304) inserted in the MTX vacuum vessel on June 21, 1990. The source has a half-life of 2.65 years and its strength was 1 mCi on November 30, 1989. The source strength on the day of the calibration should have been 3.71×10^6 neutrons/sec (n/s). The neutron source was located on the plasma axis at ports B, D, and F. Both ports D and F are 120° away from port B. Figure 15 shows the calibration data of the B-1 detector, which is the same efficiency as the A-1 detector. In this figure, the toroidal angle θ is the angle along the plasma axis between port B and source position. It is impossible to get a fitting curve for a calculation of detection efficiency from these three data points. We evaluate the efficiency of the A-1 detector based on a simple model calculation using this calibration data of the B-1 detector.

The source emits neutrons uniformly in every direction. The neutron flux should decrease in proportion to the square of the distance from the source, if the effects of scattering and absorption are not considered. Figure 16 is a schematic diagram of the geometry showing the source position and the detector position. The distance l is written as

$$l^2 = h^2 + R^2 + (R+d)^2 + 2R(R+d)\cos\theta \quad , \tag{1}$$

where θ is a toroidal angle between the detector port and the neutron source port. The length R is the major radius; h and d are the horizontal and vertical lengths between the plasma axis and the detector. The dotted lines in Fig. 15 are $1/l^2$ curves normalized at the toroidal angle θ=0° and θ=120°. These two different curves mean that the neutron flux decreases not only by distance but also by some

other factors. The neutrons from the inside vacuum vessel penetrate thick copper plates and a liquid nitrogen wall in the MTX tokamak. They should be reduced there. Around θ=0°, neutrons come through almost directly without any reduction. Increasing θ, neutrons are reduced by copper plates and liquid nitrogen. Therefore we estimate the average calibration factor from these two $1/l^2$ curves under the assumption that the efficiency curve jumps down from one to the other at the toroidal angle $\theta=\theta_c$. Table 5 gives the calculated efficiency η_1 of the A-1 detector for various θ_c. The uncertainty in the calibration is a factor of two due to the uncertainty in selecting θ_c between 5° and 30°.

Figure 17 shows the relative efficiency of the A-1 detector and the A-2 detector. The plot shows detector count rate in a standard ohmic plasma. The straight line shows that the relative efficiency η_1/η_2=3.5 obtained from the in situ calibration is consistent with the plasma data in the region of 5×10^3 ~ 5×10^4 counts/sec (cps) for the A-1 detector count rate.

We can see that the saturation count rate of the A-1 detector is 50 kcps in Fig. 17. Then we choose these two detector ranges as follows

$$\begin{aligned} N_m &= c_1 \cdot N_1 && \text{if } N_1 < 2\times10^4 \text{ cps,} \\ N_m &= \frac{1}{2}\left(c_1 \cdot N_1 + c_2 \cdot N_2\right) && \text{if } 2\times10^4 \le N_1 \le 5\times10^4 \text{ cps,} \\ N_m &= c_2 \cdot N_2 && \text{if } N_1 > 5\times10^4 \text{ cps,} \end{aligned} \qquad (2)$$

where N_m is the measured thermonuclear neutron rate and N_1 and N_2 are the count rates of detector A-1 and A-2, respectively. The calibration factor c_1 is the reciprocal of the efficiency η_1. The calibration factor c_2 is the product of the relative efficiency η_1/η_2 and c_1. We set the efficiency $\eta_1=3\times10^{-6}$ corresponding to the value of θ_c=15°. Then the calibration factors are

$$c_1 = 3.3\times10^5,$$

$$c_2 = 11.6\times10^5.$$

2.3 Calculation of ion temperature

The thermonuclear neutron rate N from a Maxwellian plasma can be written as a function of the ion temperature and the deuteron density as the following

equation:

$$N = 4\pi R \int_0^a \frac{1}{2} n_D(r)^2 <\sigma v> r\, dr\ , \tag{3}$$

where $<\sigma v>$ is the reaction rate averaged over the ion Maxwellian distribution function, and

$$<\sigma v> = \frac{\alpha_1}{T_i(r)^{2/3}} \left[1 + \alpha_2\, T_i(r)^{\beta}\, exp\left(- \frac{\alpha_3}{T_i(r)^{1/3}} \right) \right], \tag{4}$$

$\alpha_1 = 2.72\times10^{-14}$,
$\alpha_2 = 5.39$,
$\alpha_3 = 19.8$,
$\beta = 0.917$,
a = 0.165 m (minor radius),
R = 0.64 m (major radius),
$n_D(r)$ is the deuterium density in m^{-3},
$T_i(r)$ is the ion temperature in keV.

Figure 18 shows the calculated total neutron rate as a function of the central ion temperature. In this calculation, the deuteron density profile and the ion temperature profile were taken to be

$$n_D(r) = n_D \left[1 - \left(\frac{r}{a} \right)^2 \right]\ , \tag{5}$$

$$T_i(r) = T_i \left[1 - \left(\frac{r}{a} \right)^2 \right]^2\ , \tag{6}$$

n_D is the central peak deuterium density,
T_i is the central peak ion temperature.

By substituting Eq. (5) into Eq. (3), the neutron rate in Eq. (3) becomes a function of the central deuteron density n_D^2. We can then introduce a normalized neutron rate N_n at $n_D = 1\times10^{20}$ m^{-3} as

$$N_n = \frac{N}{n_{D[20]}{}^2} = 4\pi R \left(1\times10^{20} \right)^2 \int_0^a \frac{1}{2} <\sigma v> r \left[1 - \left(\frac{r}{a} \right)^2 \right] dr\ , \tag{7}$$

where $n_{D[20]} = \dfrac{n_D}{1\times10^{20}}$.

Then N_n is a function of only the ion temperature. Equation (7) can be approximated by a convenient form

$$N_n = p \cdot T_i^q , \tag{8}$$

where coefficients p and q vary with the range of N_n. Table 6 gives the parameters in the range of N_n=1×10^7 ~ 1×10^{12} n/s. The difference between Eq. (7) and Eq. (8) is within 10 eV for T_i<1 keV, and within 20 eV for T_i>1 keV.

From Eq. (8), the ion temperature can be written

$$T_i = \left(\frac{N_n}{p} \right)^{\frac{1}{q}} . \tag{9}$$

Parameters $1/p$ and $1/q$ are also shown in Table 6. Here we assume that the deuterium density is the same as the electron density and that the profile is given by Eq. (5). Therefore the central deuteron density n_D is 1.5 times the line-averaged electron density from the FIR central chord:

$$n_D = 1.5 \times \overline{n_e} .$$

We can obtain the measured thermonuclear neutron rate N_m from the neutron measurement given in Eq. (2). Then the ion temperature is obtained from the measured thermonuclear neutron rate and the line-averaged electron density as follows,

$$T_i = \left(\frac{N_m / {n_{D[20]}}^2}{p} \right)^{\frac{1}{q}} . \tag{10}$$

Using this form, we can then calculate the ion temperature for each plasma shot by combining the FIR data through the VAX computer.

2.4 Neutron production rate and ion temperature

Figures 19and 20 show the time evolution of typical MTX plasma parameters and the total neutron production rates for the shot No. 7794 on March 28, 1990. In Fig. 20 the open circles shows the neutron measurement data and the closed circles show the calculated data from the neoclassical transport study by M. M. Marinak. The calibration factor is calculated assuming θ_c=15°±5°. The uncertainty of the neutron data in Fig. 20 comes from only that of this calibration

factor.

Figure 21 shows the trend of central electron and ion temperature with central peak electron density at the toroidal magnetic field B_t=8 T and the plasma current I_p=250~400 kA. The central electron temperatures and densities were obtained from the Thomson scattering system. The ion temperatures obtained from the neutron production rate are found to be smaller than the electron temperature by about 0.2 keV. The electron temperature decreases as the electron density increases, but the ion temperatures are almost constant above $n_e>2\times10^{20}$ m^{-3}.

Here we discuss an uncertainty of the ion temperature deduced from neutron emission. In Eq. (10), the error comes from the uncertainty in the measured thermonuclear neutron rate, the uncertainty in the deuteron density and its profile, and the uncertainty in the temperature profile arising from its factors p and q. Figure 22 shows the variation of the central ion temperature calculated from neutron rates and its dependence on the profiles of the temperature and the density at the central deuteron density $n_D=1\times10^{20}$ m^{-3}. In this figure, i_T and i_n are the temperature and the density profile parameters:

$$T_i(r) = T_i\left[1-\left(\frac{r}{a}\right)^2\right]^{i_T}, \tag{11}$$

$$n_D(r) = n_D\left[1-\left(\frac{r}{a}\right)^2\right]^{i_n}, \tag{12}$$

a is the plasma radius.

These calculations show that the change in the central ion temperature between i_T=1 and i_T=2 is no more than 75 eV when near the central ion temperature T_i=1 keV.

The uncertainty in the deuteron density is rather complicated. If we know the central deuterium density, the error from the profile is very small, within 25 eV as shown in Fig. 22. However, the error may be large when the deuterium density is deduced from the line-averaged electron density measurement. The deuterium density is usually not equal to the electron density because of impurity contamination in the plasma. Here we assume the ions in the plasma consist of deuteron, hydrogen and eighth ionized oxygen. Then the ratio of deuteron density and electron density is

$$\xi = \frac{n_D}{n_e} = \frac{8 - Z_{eff}}{7 \cdot (1 + \zeta)} \quad , \tag{13}$$

where ζ is the ratio of the hydrogen and deuterium, and Z_{eff} is the effective charge, these parameters defined by

$$\zeta = \frac{n_H}{n_D} , \tag{14}$$

$$Z_{eff} = \frac{\sum_{\alpha} n_\alpha \cdot Z_\alpha{}^2}{\sum_{\alpha} n_\alpha \cdot Z_\alpha} , \tag{15}$$

n_α is the density of particle α and

Z_α is the charge of particle α.

Figure 23 shows how the ratio of the deuteron to the electron density depends on the variables ζ and Z_{eff}. The ratio is 0.9 at Z_{eff}=1.7, if the contamination of hydrogen can be neglected. Under an assumption of the uniformity of Z_{eff}, ζ, and ξ in space, the deuteron line-averaged density is

$$\overline{n_D} = \xi \cdot \overline{n_e} \quad , \tag{16}$$

and the central peak deuteron density is

$$n_D = k_n \cdot \overline{n_D} \quad , \tag{17}$$

where k_n is the coefficient of the density profile and is

$$k_n = \frac{3}{2} \qquad \text{if } i_n = 1 ,$$

$$k_n = \frac{15}{8} \qquad \text{if } i_n = 2 .$$

The error in the central deuteron density is due to the uncertainty of the density ratio ξ, the density profile coefficient k_n and the measured electron density. The range of the density ratio is ξ=0.7 to ξ=0.9 corresponding to Z_{eff}=1.5~3.0. And the range of the density profile coefficient is k_n=1.5 to k_n=1.9, corresponding to i_n=1~2. The uncertainty in the central deuteron density from the electron density measurement is 1.6 from these calculations, if the uncertainty of the measured electron density can be neglected.

The error in the measured total neutron rate is due to the uncertainty in the calibration factor and the statistics of the detector count rate. The calibration factor has the uncertainty of roughly a factor of two already discussed in Sec. 2.2. The error due to the counting statistics is only 10 % because the typical count rate is 100 counts with 5 ms sampling time. That is negligible compare with the calibration factor. The normalized neutron rate of the A-1 detector is represented by

$$N_n = \frac{c_1}{(k_n \cdot \xi)^2} \cdot \frac{N_1}{\overline{n_e}^2} \ . \tag{18}$$

The range of the denominator of the coefficient in Eq. (18) is 1.1~2.9. The range of coefficient c_1 is $2.4\times10^5 \sim 4.5\times10^5$ from Table 5, in which the coefficient c_1 is the reciprocal of the efficiency η_1. Then the range of the coefficient of normalized neutron rate is $8.2\times10^4 \sim 4.1\times10^5$. When N_1=20 kcps and $\overline{n_e}^2=1\times10^{20}$ m^{-3}, the normalized neutron rate is $1.6\times10^9 \sim 8.2\times10^9$ n/s, which corresponds to the range of the ion temperature 0.7~1.0 keV, including the uncertainty in the temperature and density profile.

We conclude that the error range of the ion temperature is ±0.15 keV for T_i near 1 keV. This uncertainty reduces to ±0.10 keV, which comes from the uncertainty of the calibration factor, when we know the density profile and Z_{eff}.

3. High-speed neutron measurement

A high temporal resolution is required to observe the ion response to a microwave pulse from the FEL. A plastic scintillator (NE102A) with a nanosecond response was used for neutron detection.

3.1 Measurement system

The uncollimated scintillator, which was 5 cm in diameter and 10 cm in length, was inserted into the MTX top port and placed 48 cm above the horizontal plane of the plasma center. The NE102A plastic scintillator has a 2.4 ns decay time constant, and the output pulse through the amplifier typically has a 7 ns rise time and 15 ns FWHM. The original system used a 20 m fiber bundle to transmit the photon signal to the photomultiplier tube, as shown in Fig. 24. The

The error in the measured total neutron rate is due to the uncertainty in the calibration factor and the statistics of the detector count rate. The calibration factor has the uncertainty of roughly a factor of two already discussed in Sec. 2.2. The error due to the counting statistics is only 10 % because the typical count rate is 100 counts with 5 ms sampling time. That is negligible compare with the calibration factor. The normalized neutron rate of the A-1 detector is represented by

$$N_n = \frac{c_1}{(k_n \cdot \xi)^2} \cdot \frac{N_1}{\overline{n_e}^2} \ . \tag{18}$$

The range of the denominator of the coefficient in Eq. (18) is 1.1~2.9. The range of coefficient c_1 is $2.4\times10^5 \sim 4.5\times10^5$ from Table 5, in which the coefficient c_1 is the reciprocal of the efficiency η_1. Then the range of the coefficient of normalized neutron rate is $8.2\times10^4 \sim 4.1\times10^5$. When N_1=20 kcps and $\overline{n_e}^2=1\times10^{20}$ m^{-3}, the normalized neutron rate is $1.6\times10^9 \sim 8.2\times10^9$ n/s, which corresponds to the range of the ion temperature 0.7~1.0 keV, including the uncertainty in the temperature and density profile.

We conclude that the error range of the ion temperature is ±0.15 keV for T_i near 1 keV. This uncertainty reduces to ±0.10 keV, which comes from the uncertainty of the calibration factor, when we know the density profile and Z_{eff}.

3. High-speed neutron measurement

A high temporal resolution is required to observe the ion response to a microwave pulse from the FEL. A plastic scintillator (NE102A) with a nanosecond response was used for neutron detection.

3.1 Measurement system

The uncollimated scintillator, which was 5 cm in diameter and 10 cm in length, was inserted into the MTX top port and placed 48 cm above the horizontal plane of the plasma center. The NE102A plastic scintillator has a 2.4 ns decay time constant, and the output pulse through the amplifier typically has a 7 ns rise time and 15 ns FWHM. The original system used a 20 m fiber bundle to transmit the photon signal to the photomultiplier tube, as shown in Fig. 24. The

photomultiplier tube (R329-02) has a fast time response, typically with 2.5 ns rise time; the most sensitive wavelength is 420 nm, which is optimum for the plastic scintillator. Figure 25 shows the electronics circuit. This scintillator probe with the OKEN Pulse & DC amplifier can operate in both the pulse-count mode and current mode shown in Fig. 26. The amplifier has fast frequency response, 16 MHz in pulse output and 160 kHz in direct current output. The pulse outputs through the OKEN 805-1 discriminator connected to the CAMAC eight-channel scaler, which also was connected to the proportional counters and the fission counters. The OKEN 714-1E supplies the PMT bias voltage up to ±2 kV. This scintillator probe requires negative voltage. The detection efficiency of this system depends on the PMT high voltage and the discriminator threshold voltage in the pulse-count mode operation. The optimum PMT voltage V_{PMT}=-1.7 kV and threshold voltage of the discriminator V_{TH}=-200 mV were determined from plasma shot data by comparing ^{3}He counter signals. The time resolution of this system for standard ohmic plasmas was about 1 kHz, limited by counting statistics. The transmission of the fiber bundle is not optimum for the photons from the plastic scintillator. The calculated total transmission efficiency of the fiber bundle was only 38% at 420 nm wavelength. Therefore, we redesigned this system using a long acrylic light guide instead of a fiber bundle to transmit the photon signal to a photomultiplier, as shown in Fig. 27. The photomultiplier tube was located at 1.25 m above the top port, where the stray magnetic field was weak enough to be eliminated with a 10-mm-thick magnetic shield. Figure 28 shows the electronic circuit for this modified system. The OKEN 803-2 preamplifier was used instead of the S-1906 to make the system compact. This circuit can operate only in pulse-count mode. This modified scintillator probe requiers positive bias voltage, which is opposed to the original system. Using this modified system, we could decrease the transmission loss and obtain better counting statistics. The temporal resolution was up to 2 kHz for standard ohmic plasmas.

3.2 Response for deuterium pellet

Figure 29 shows the time evolution of the plasma current, the line-averaged electron density, the neutron emission, and the hard x-ray in a pellet injection experiment. The neutron signal comes from the plastic scintillator with 1 ms of sampling time in the pulse-count mode. The neutron signal has a large spike in the start phase of the discharge. The hard x-ray signal shows that this spike comes from intense x-ray emission. One deuterium pellet is injected into the

plasma at 0.26 s in this discharge. The neutron emission drops initially at the time of pellet injection because of a decrease in the temperature. A soft x-ray signal shows the abrupt drop of the electron temperature caused by cold particles from the evaporating pellet. The neutron rate then increases as the temperature recovers and becomes five times higher than the original value at about 40 ms after the pellet injection in this discharge.

4. Summary

Two types of neutron measurement systems were installed and operated in the MTX tokamak. The proportional counter system was absolutely calibrated using a ^{252}Cf source. The calibration was carried out in the unsuitable configuration of the MTX tokamak. The uncertainty of the neutron rate is roughly a factor of two. However, the uncertainty of the ion temperature deduced from the neutron measurement is within ±0.15 keV because of the strong ion temperature dependence of the neutron rate. The total neutron production was evaluated from the neutron measurements and found consistent with the calculation from the neoclassical transport study. This measurement system could operate as designed over the wide dynamic range of neutron rate from 10^8 n/s to possibly 10^{13} n/s. The central ion temperature was estimated from the neutron measurements using the FIR electron density data.

The plastic scintillator system for high-speed measurements made fast-time-response measurements on pellet injected plasmas. We did not see any response to the 1-GW-level single FEL pulses during physics studies of the MTX plasma. We tried to increase the sampling clock frequency up to 10 kHz. The temporal resolution of 10 kHz was not fast enough to detect the response to the very short FEL pulse. It would have been possible to obtain better counting statistics with faster sampling time in pulse-count mode by collection of data from more than one discharge of the same type. Unfortunately, further experiments were not performed due to time constraints.

Experiments on MTX were concluded in July, 1992 and the MTX project was shut down at the end of the 1992 fiscal year. Almost all pieces of equipment supplied by JAERI, including the neutron diagnostic, were removed from MTX in September, 1992 and were returned to JAERI in December, 1992.

plasma at 0.26 s in this discharge. The neutron emission drops initially at the time of pellet injection because of a decrease in the temperature. A soft x-ray signal shows the abrupt drop of the electron temperature caused by cold particles from the evaporating pellet. The neutron rate then increases as the temperature recovers and becomes five times higher than the original value at about 40 ms after the pellet injection in this discharge.

4. Summary

Two types of neutron measurement systems were installed and operated in the MTX tokamak. The proportional counter system was absolutely calibrated using a ^{252}Cf source. The calibration was carried out in the unsuitable configuration of the MTX tokamak. The uncertainty of the neutron rate is roughly a factor of two. However, the uncertainty of the ion temperature deduced from the neutron measurement is within ±0.15 keV because of the strong ion temperature dependence of the neutron rate. The total neutron production was evaluated from the neutron measurements and found consistent with the calculation from the neoclassical transport study. This measurement system could operate as designed over the wide dynamic range of neutron rate from 10^8 n/s to possibly 10^{13} n/s. The central ion temperature was estimated from the neutron measurements using the FIR electron density data.

The plastic scintillator system for high-speed measurements made fast-time-response measurements on pellet injected plasmas. We did not see any response to the 1-GW-level single FEL pulses during physics studies of the MTX plasma. We tried to increase the sampling clock frequency up to 10 kHz. The temporal resolution of 10 kHz was not fast enough to detect the response to the very short FEL pulse. It would have been possible to obtain better counting statistics with faster sampling time in pulse-count mode by collection of data from more than one discharge of the same type. Unfortunately, further experiments were not performed due to time constraints.

Experiments on MTX were concluded in July, 1992 and the MTX project was shut down at the end of the 1992 fiscal year. Almost all pieces of equipment supplied by JAERI, including the neutron diagnostic, were removed from MTX in September, 1992 and were returned to JAERI in December, 1992.

Acknowledgments

The authors would like to acknowledge the MTX members at LLNL for operations and maintenance of the tokamak, measurements of several plasma parameters, and developments of the FEL. We would like to thank a few in particular.

Bradley Rice and Robert Geer made significant contributions to the installation of the detection electronics on MTX. Craig Brooksby did the design and fabrication of the support stands of the neutron moderator. William Meyer was invaluable in the installation and the maintenance of the computer system, and also in supplying the display and analysis programs for data acquisition. Dave Nilson contributed to the calibration of the detectors using neutron sources. Tom Casper and Bradley Rice worked on the FIR interferometer measurement that gave the temporal behavior of the electron density. Thomson scattering measurements were obtained by James Foote and John Jolly. Martin Marinak calculated neutron rates using the neoclassical transport code. And the MTX tokamak was operated by Reginald Wood, Steven Allen and Charles Lasnier.

We thank Thomas Casper for his leadership in diagnostics, and Edwin Hooper and Steven Allen for their useful discussions. We are also grateful to James Foote who carefully read the manuscript and suggested numerous improvements.

This work was performed under the DOE-JAERI collaborative program for the MTX project and by the Lawrence Livermore National Laboratory for U.S. DOE under Contract No. W-7405-ENG-48.

REFERENCES

1) Thomassen K.I. : "Free-Electron Laser Experiments in Alcator C", LLL-PROP-00202 (1986).
2) Jong R. A. , Stone R. R. : Nucl. Instrum. Methods, A285, 387 (1989).
3) Nevins W. M. , Rognlien T. D. , and Cohen B. I. : Phys. Rev. Lett. 59, 60 (1987).
4) Felker B. and Ferguson S. W. : Proc. of the 14th IEEE-NPSS Fus. Eng. Symp. (San Diego), 132 (1991) .
5) Fisher W. A. : PFC/RP-83-3 (1983).
6) Casper T. , Allen S. , Foote J. , Fenstermacher M. , Hooper E. , Hoshino K. et al : Rev. Sci. Instrum. , 61 (10) , 3274 (1990)
7) Jong R. A. , Atkinson D. P. , Byers J. A. , Coffield F. E. , Deis G. A. , et al : Nucl. Instrum. Methods, A285, 379 (1989).
8) Lasnier C. J. , Allen S. L. et al : "Proceedings of the 1993 Particle Accelerator Conference", Vol. 2, IEEE, 1554 (1993).
9) Allen S. L. , Brown M. D. , Byers J. A. , Casper T. A. , Cohen B. I. , et al : Plasma Physics and Controlled Nuclear Fusion Research 1990 (Proc. 13th Int. Conf. Washington D. C. , 1990), Vol. 1, IAEA, Vienna, 783 (1990).
10) Allen S. L. , Casper T. A. , Fenstermacher M. E. , Foote J. H. , Hooper E. B. , et al : Plasma Physics and Controlled Nuclear Fusion Research 1992 (Proc. 14th Int. Conf. Würzburg , 1992), Vol. 1, IAEA, Vienna, 617 (1992).
11) Allen S. L. , Brown M. D. , Byers J. A. , Casper T. A. , Cohen B. I. , et al : to be published in Phys. Rev. Lett. 72 (1994).
12) Ogawa T. , Oasa K. , Hoshino K. , Odajima K. , Maeda H. : "DESIGN OF NEUTRON DIAGNOSTIC FOR MTX", JAERI-M 90-105.
13) Ogawa T. , Oasa K. , Hoshino K. , Odajima K. , Maeda H. , The Microwave Tokamak Experimental Team : Rev. Sci. Instrum. , 61 (10) , 3181 (1990).
14) Butner D. N. , Casper T. A. , Brown M. D. , Drlik M. , Meyer W. H. and Moller J. M. : Rev. Sci. Instrum. , 61 (10) , 3277 (1990).

Table 1 Typical MTX Parameters

Tokamak	
Major Radius	0.64 m
Minor Radius	0.165 m
Toroidal Magnetic Field	5 ~ 8 T
Plasma Current	200 ~ 400 kA
Averaged Electron Density	$1 \sim 3 \times 10^{20}$ m^{-3}
Peak Electron Temperature	1 ~ 2 keV
FEL	
Electron Beam Current	2 ~ 3 kA
Electron Beam Energy	6 MeV
Electron Beam Pulse Width	30 ns
Microwave Frequency	140 GHz
Microwave Power	1 ~ 2 GW
Microwave Pulse Width	20 ~ 30 ns

Table 2 Comparison of neutron diagnostics for MTX.

Purpose	Detector	Electronics	Resolution	Merit
Neutron rate and ion temperature	Proportional counter array	Pulse count	5 ms~10 ms	Wide dynamic range High sensitivity X-ray shield
Ion behavior to FEL pulse	Plastic scintillator	Pulse count or Current mode	0.5 ms~1 ms	Fast temporal resolution

Table 3 Neutron detectors

Detector No.	Model No.	Neutron sensitive material	Fill pressure or total quantity	Active length (cm)	Diameter (cm)	Thermal neutron sensitivity (cps/nv)
1	RS-P4-1609-201	^{3}He	5 atm	22.9	5.1	80.9
2	RS-P4-0809-203	^{3}He	2 atm	22.9	2.5	19.6
3	RS-P1-0809-205	BF_3	40 cmHg	21.1	2.5	4.1
4	RS-P6-1608-110	^{235}U	1.7 grm	18.1	5.1	0.74
5	RS-P6-1608-125	^{235}U	1.7 grm	18.1	5.1	0.23

Table 4 Electronics Parameters

Detector No.	Detector Model No.	Preamp Model No.	HV Supply Model No.	HV Supply Voltage (mV)	Amp Gain	Discriminator Threshold Voltage (mV)
1	RS-P4-1609-201	TC170	TC952	+1400	250	-800
2	RS-P4-0809-203	TC170	478	+ 900	250	-800
3	RS-P1-0809-205	TC170	TC952	+1400	250	-800
4	RS-P6-1608-110	TC171	TC953	+ 800	50	-400
5	RS-P6-1608-125	TC171	TC953	+ 800	50	-400

Table 5 Detection Efficiency

θ_c	Efficiency (counts/neutron)
0°	1.76×10^{-6}
5°	2.19×10^{-6}
10°	2.60×10^{-6}
15°	3.01×10^{-6}
20°	3.42×10^{-6}
25°	3.81×10^{-6}
30°	4.19×10^{-6}

Table 6 Coefficients of neutron rate calculation

Range	p	q	$1/p$	$1/q$
$10^7 < N_n \leq 10^8$	1.91×10^{10}	8.47	5.23×10^{-11}	0.118
$10^8 < N_n \leq 10^9$	9.89×10^9	7.41	1.01×10^{-10}	0.135
$10^9 < N_n \leq 10^{10}$	7.38×10^9	6.47	1.35×10^{-10}	0.155
$10^{10} < N_n \leq 10^{11}$	7.65×10^9	5.73	1.31×10^{-10}	0.174
$10^{11} < N_n \leq 10^{12}$	1.10×10^{10}	4.92	9.10×10^{-11}	0.203

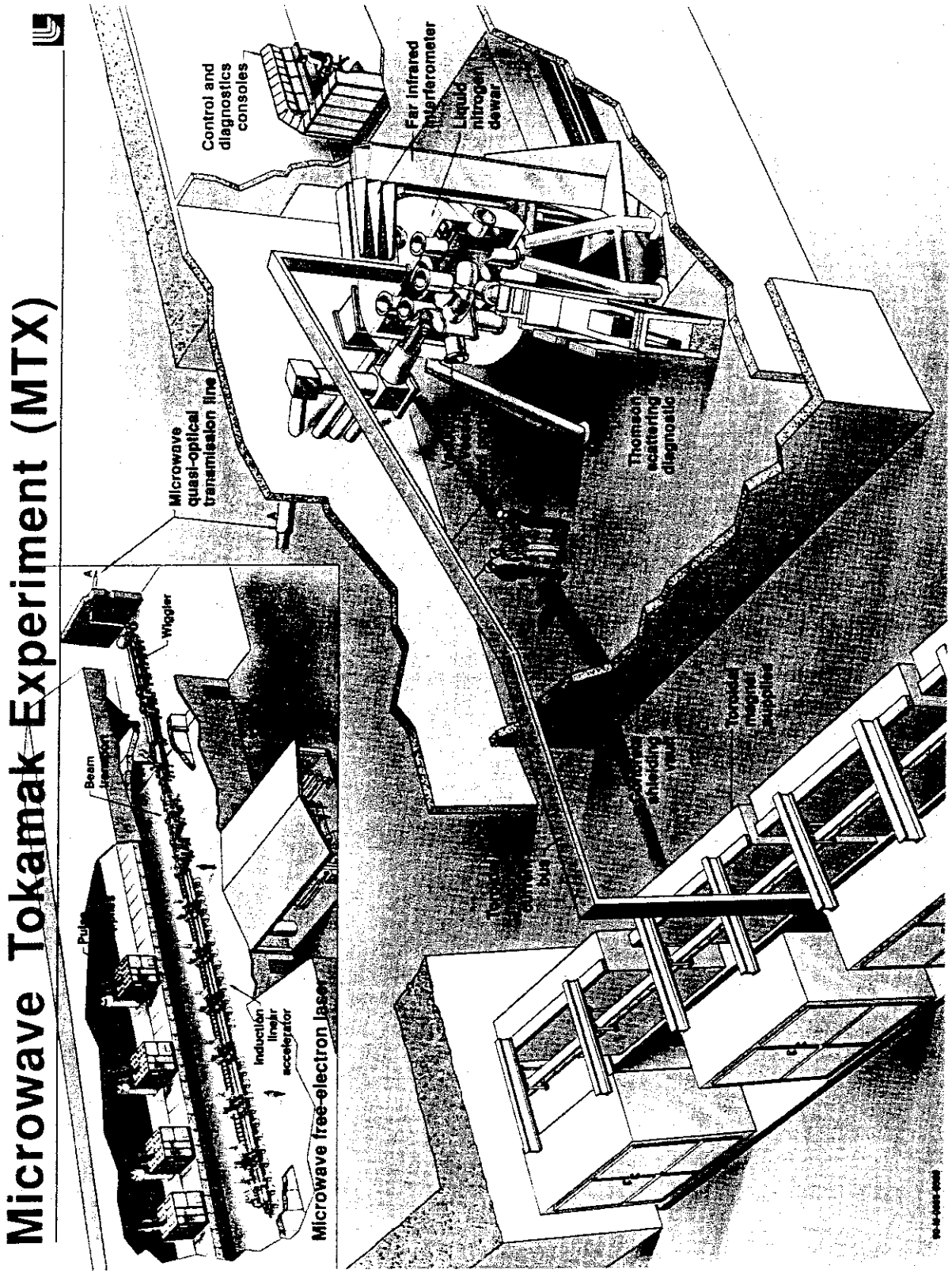

Fig.1 The components of the Microwave Tokamak Experiment, which consisted of the MTX tokamak, the free-electron laser, a quasi-optical microwave transport system, and the microwave and plasma diagnostics.

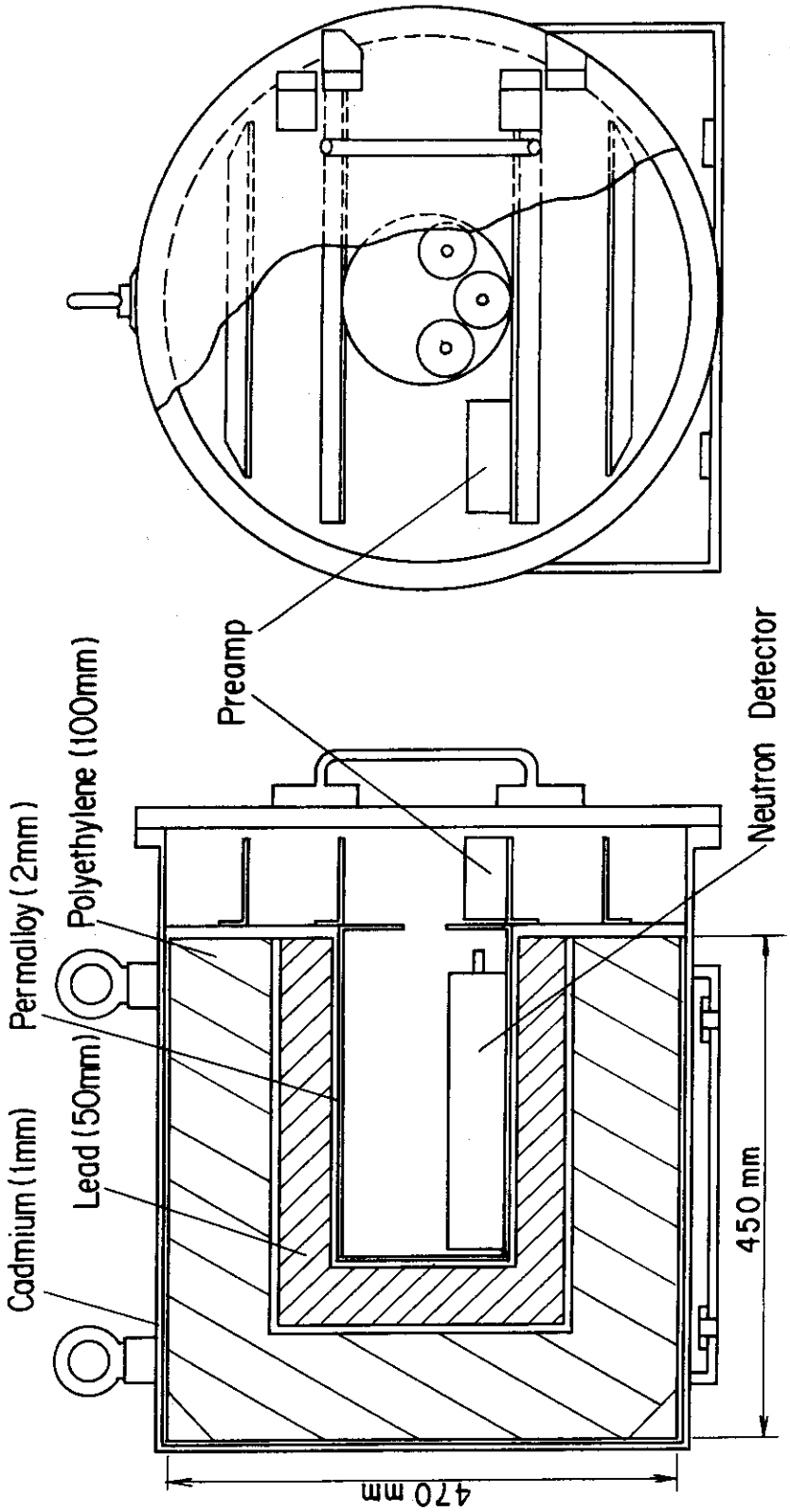

Fig. 2 Schematic diagram of the neutron moderator consisting of 100mm thick polyethylene, 50mm thick lead, 1mm thick cadmium, 2mm thick permalloy and stainless steel. Neutron detectors and preamplifiers are set together inside the neutron moderator.

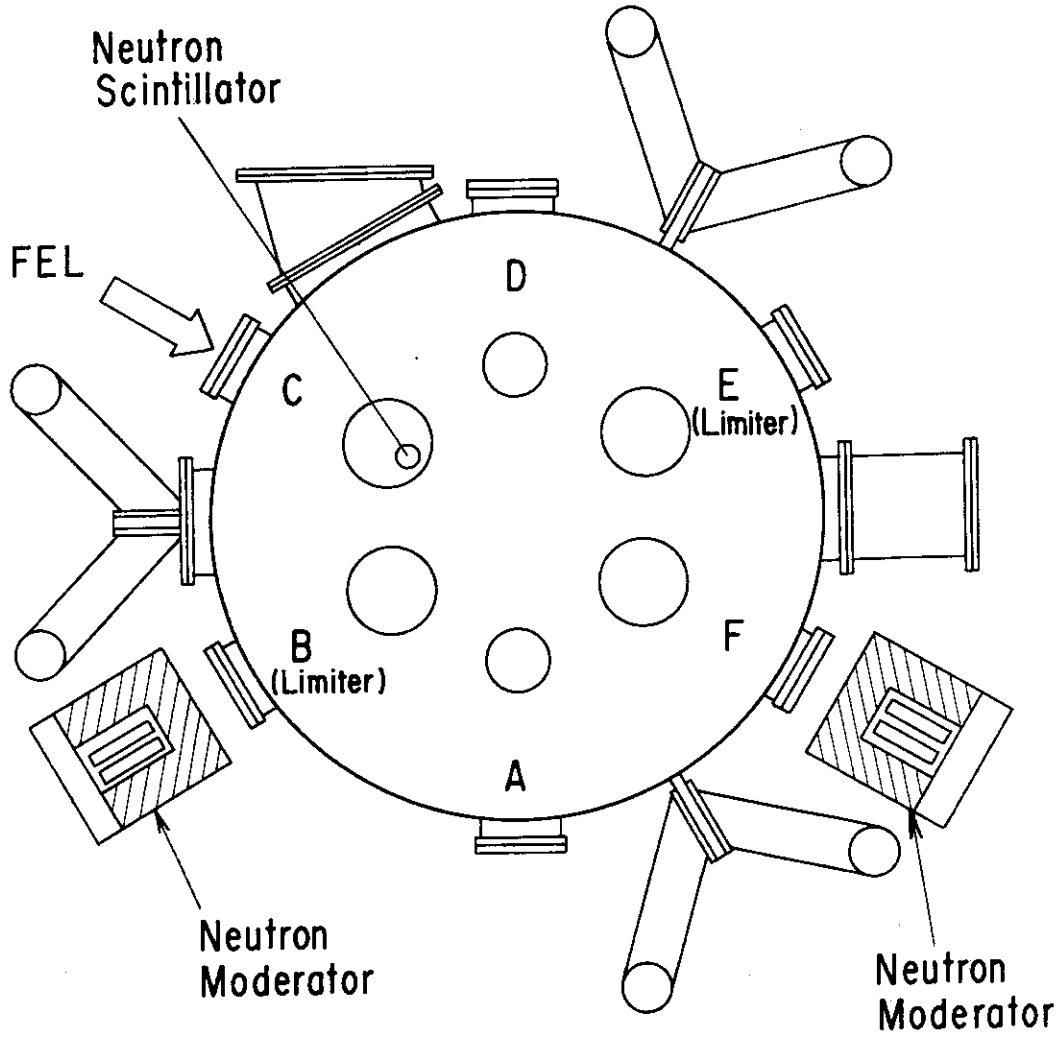

Fig.3 Schematic diagram of the MTX tokamak plan view, showing the layout of the neutron detector assemblies and the scintillator.

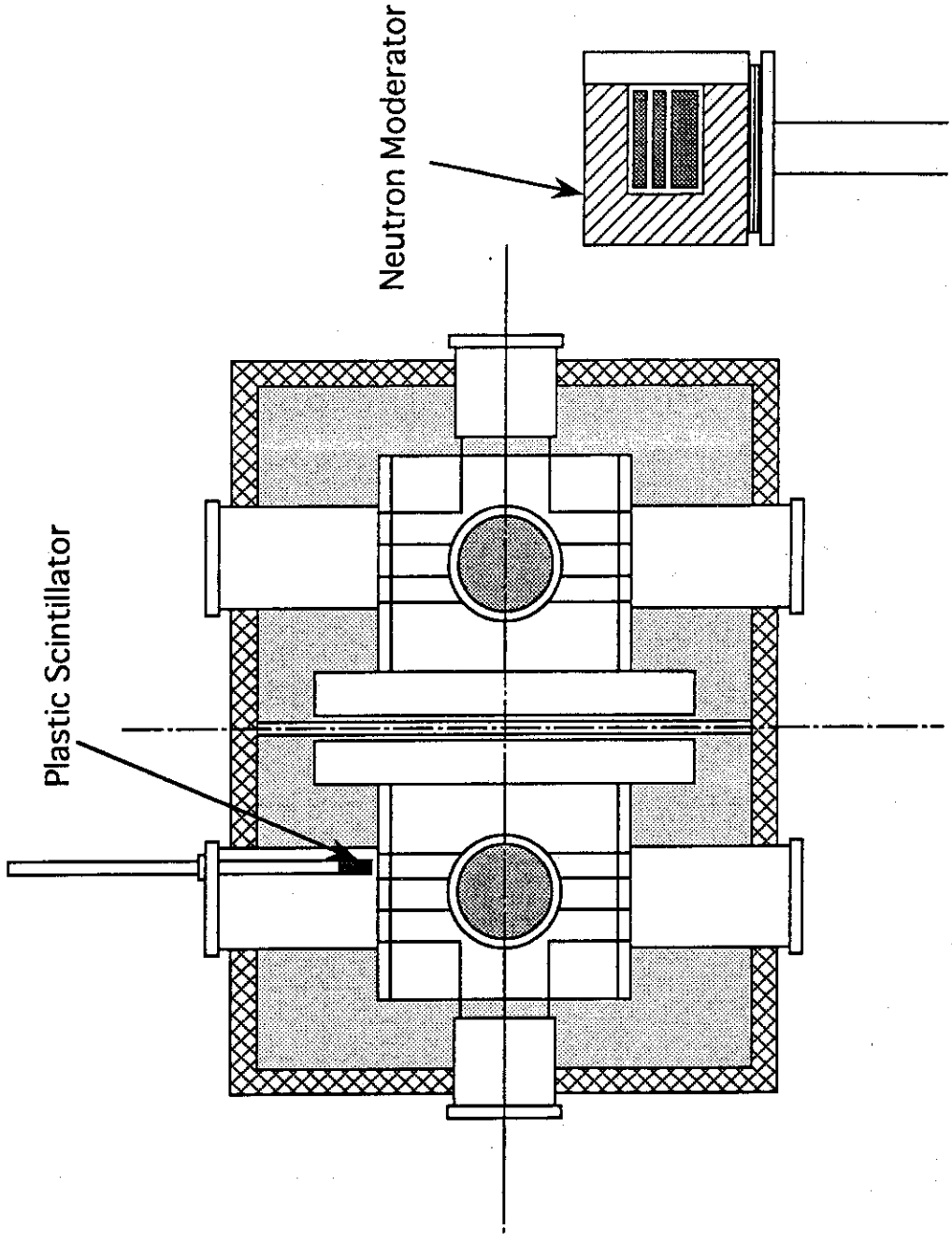

Fig.4 Elevation view of the MTX tokamak, showing the layout of the neutron detectors.

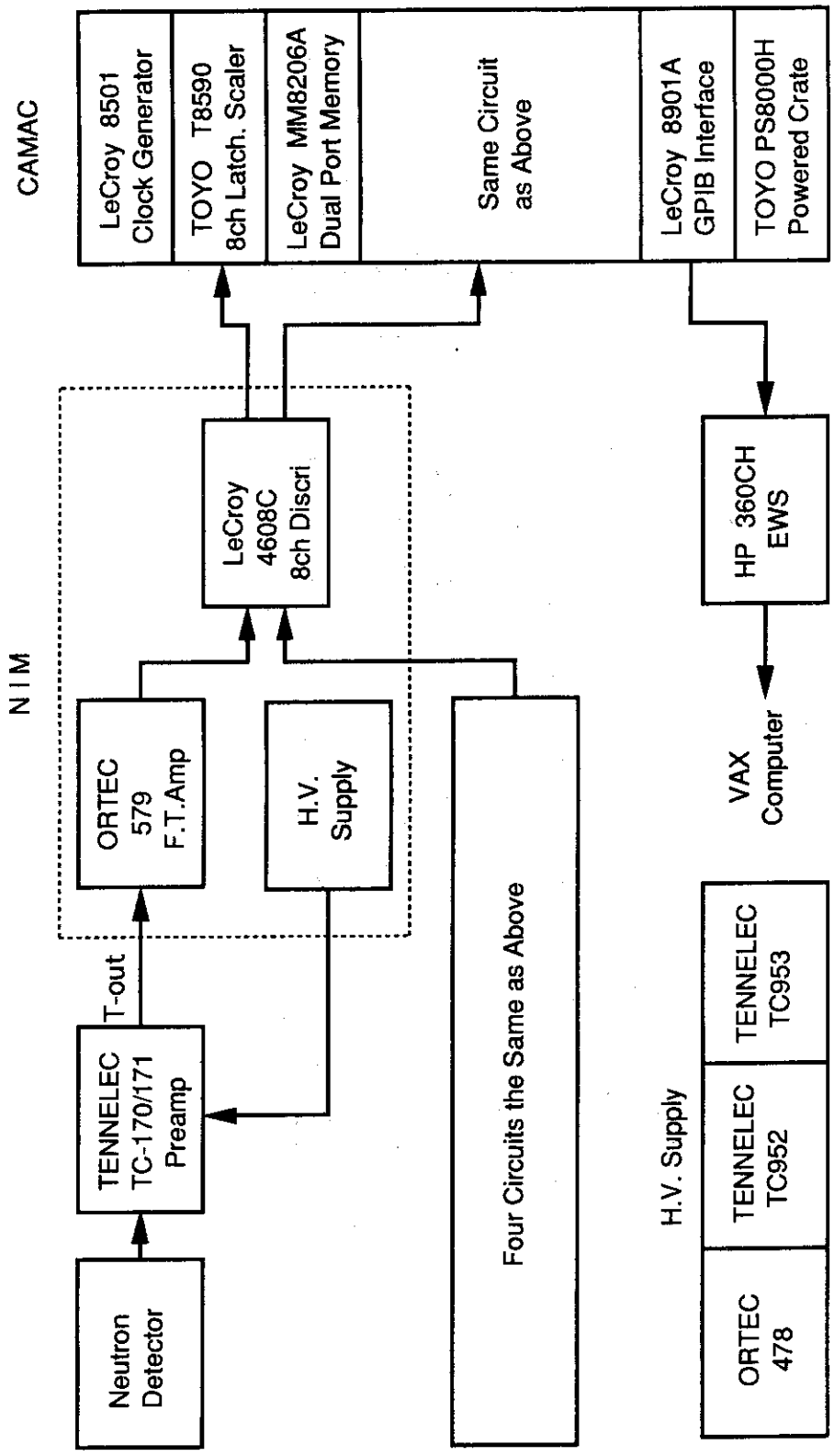

Fig.5 Electronic system for the neutron-production-rate measurement. The electronics were selected based on the requirements of high speed and high count rates capability.

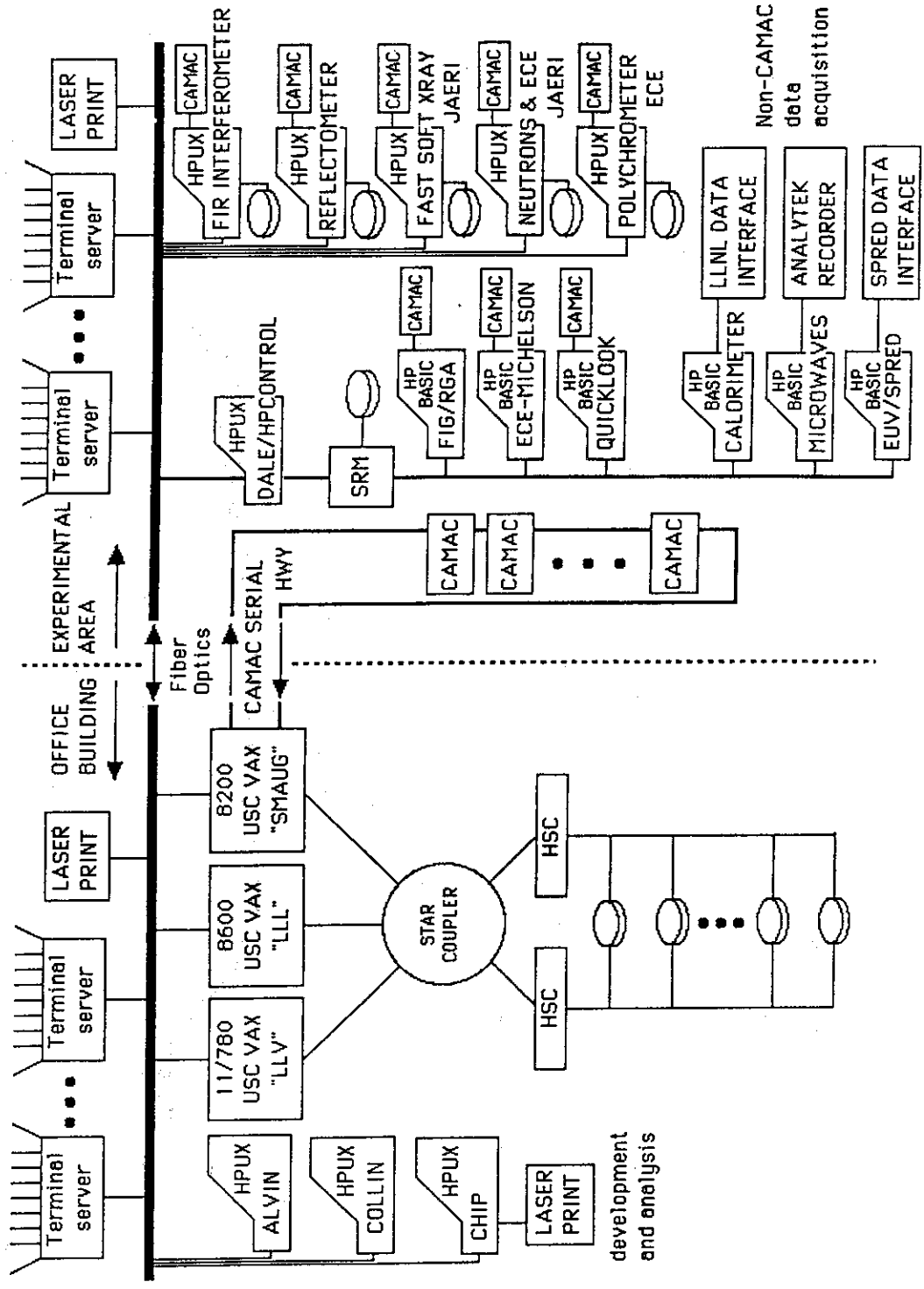

Fig. 6 Hardware configuration for the MTX data acquisition and analysis network.

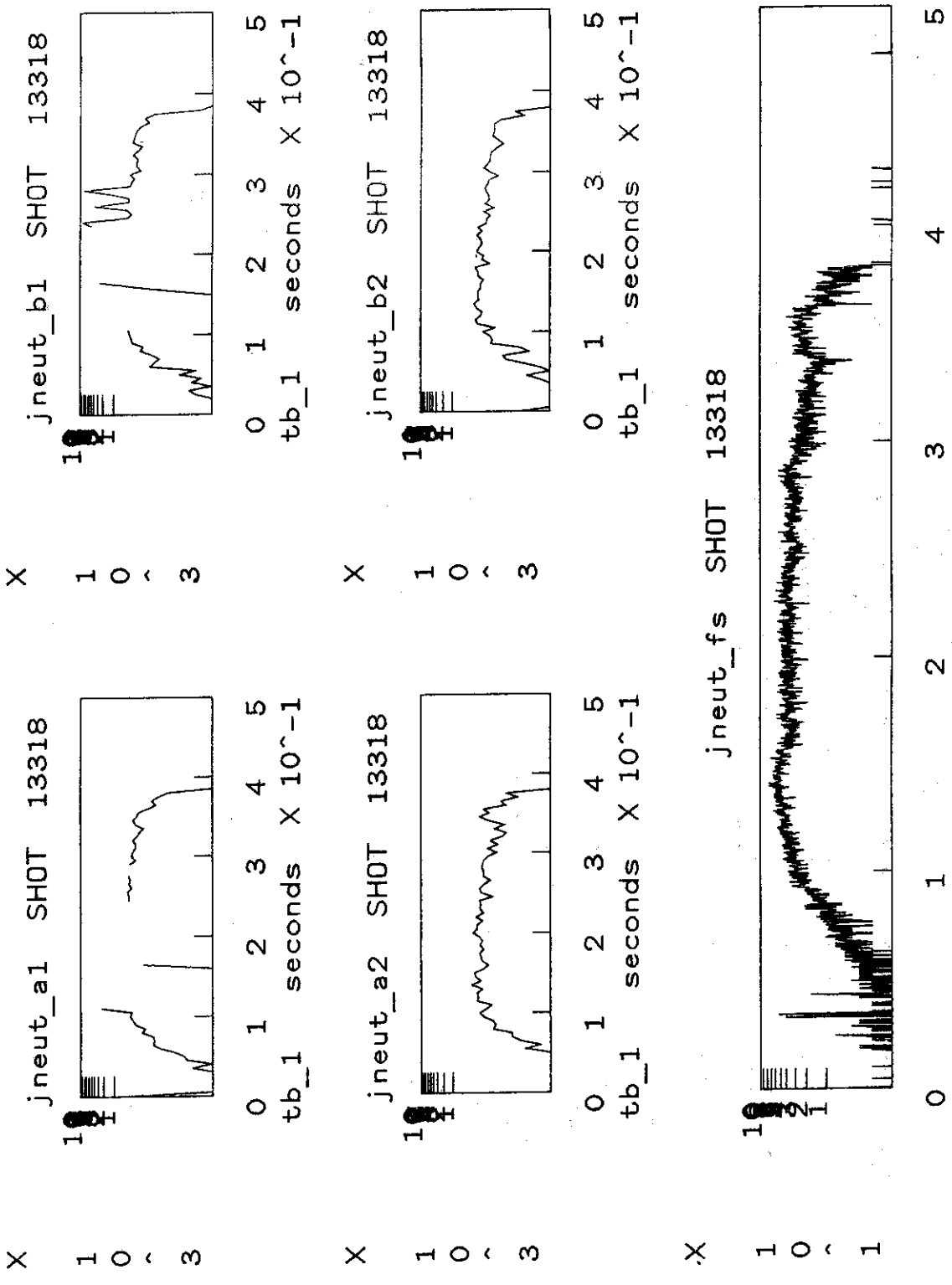

Fig. 7 (T.Ogawa)

Fig. 7 The HP 360CH computer output for the neutron diagnostic. The two most sensitive channels were usually monitored for each of the two detector arrays (A-1, A-2, B-1 and B-2). The bottom graph is the plastic scintillator data.

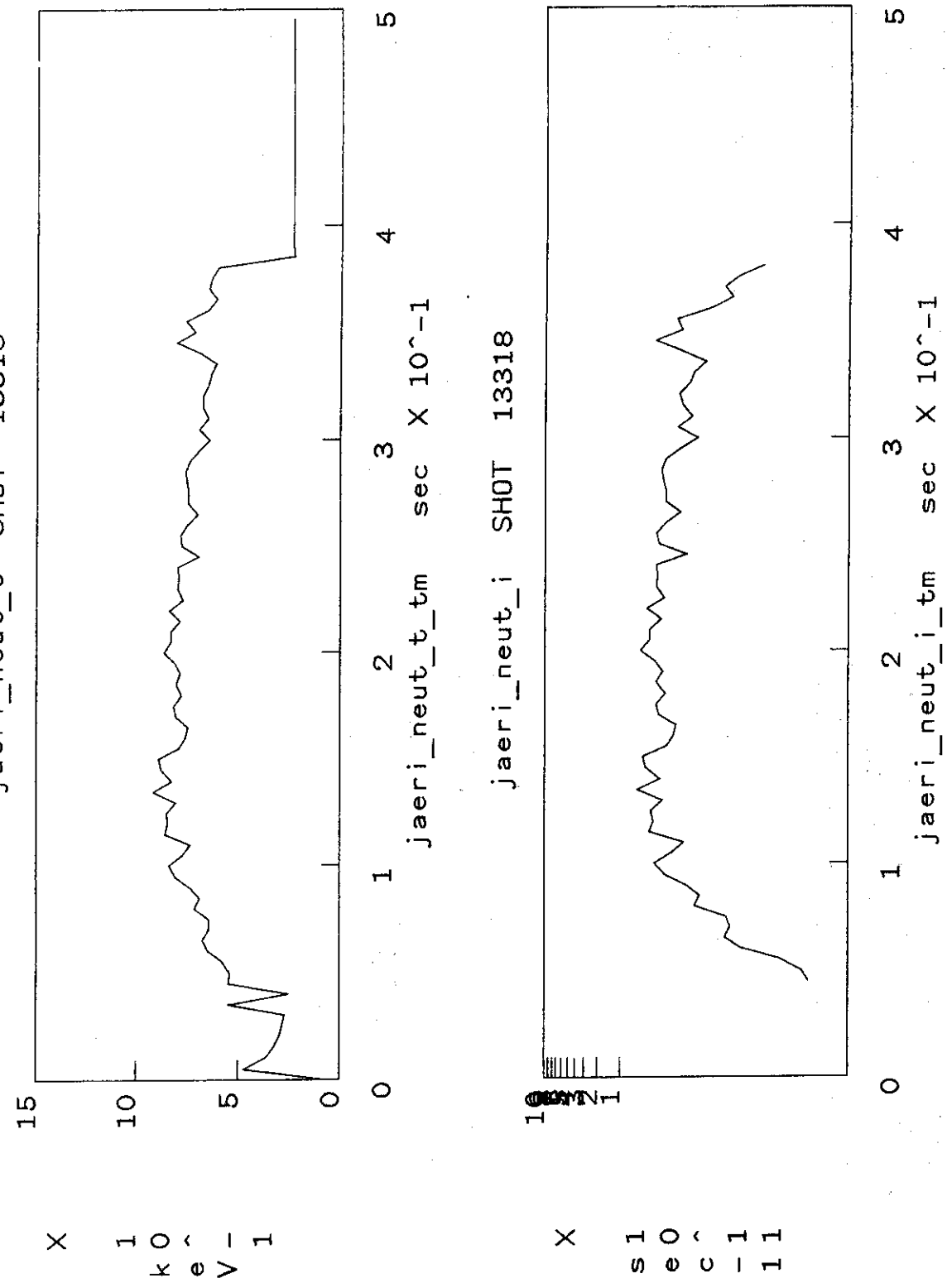

Fig.8 The HP 360CH computer output for the neutron diagnostic. The top graph is a time trace of the ion temperature and the bottom is the neutron production rate.

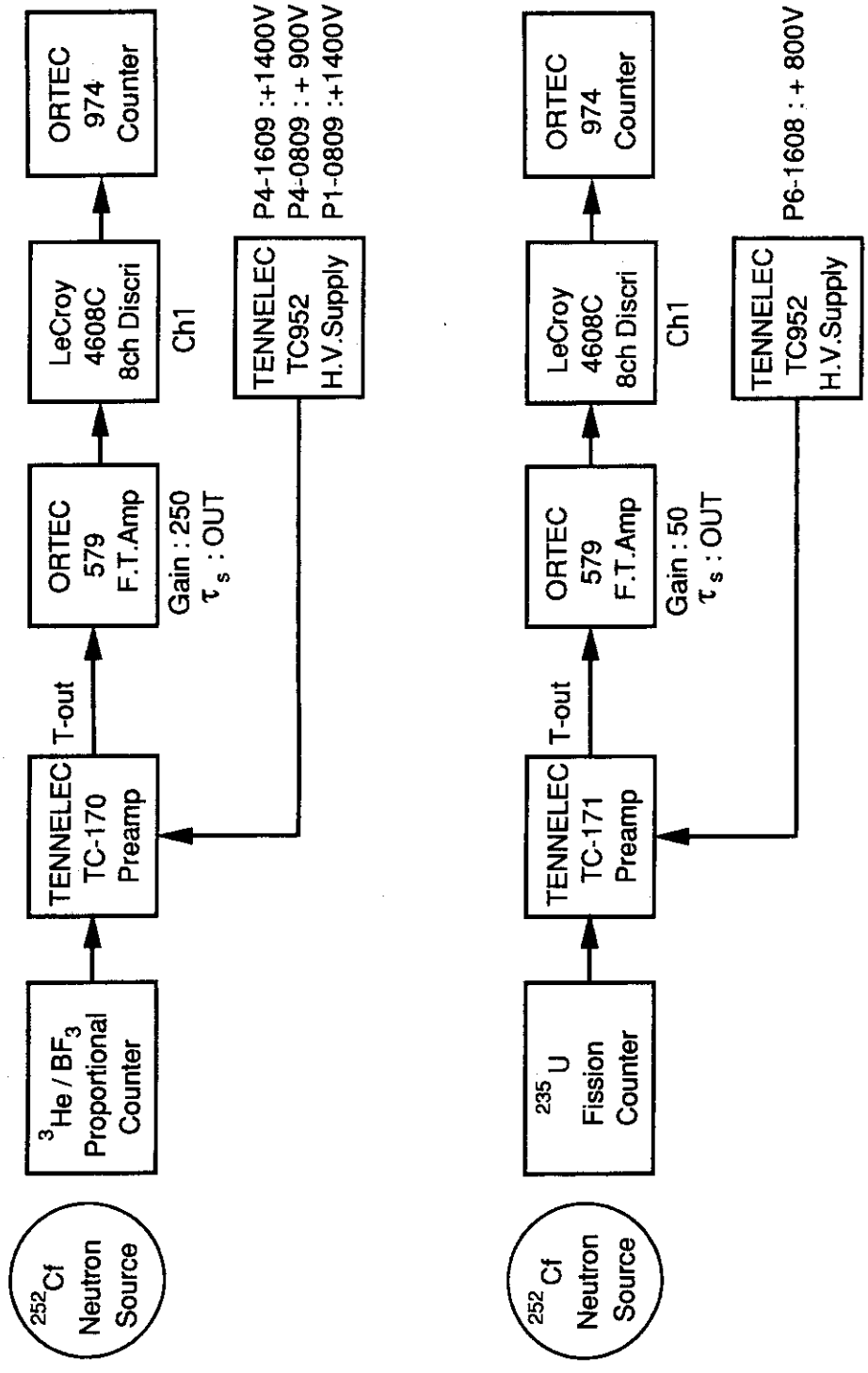

Fig. 9 Electronics circuits for detector calibration using a ^{252}Cf source.

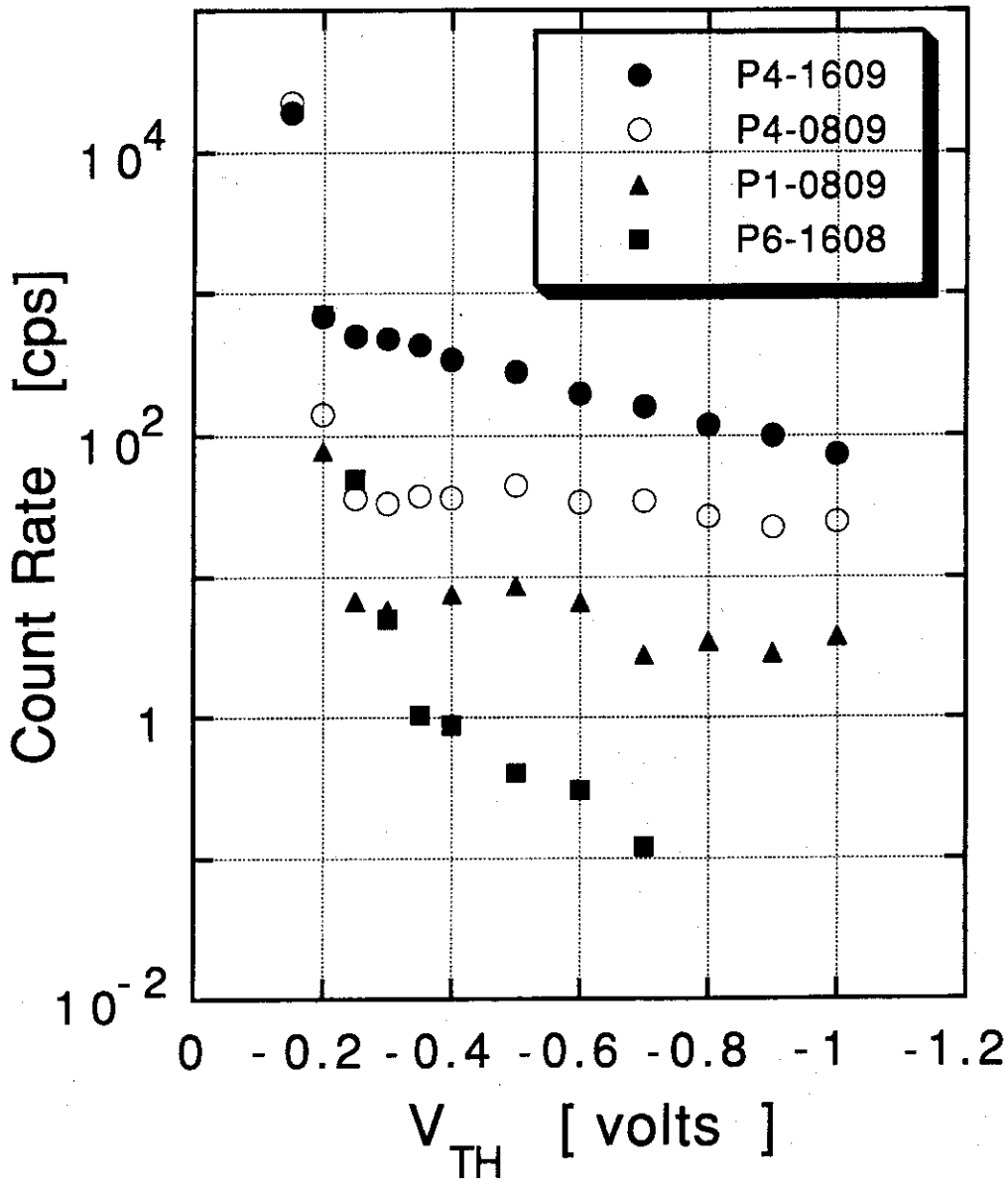

Fig. 10 The neutron count rates versus the threshold voltage on the discriminator for detector calibration. The noise rates became large below V_{TH}=-0.25V in the $^{3}H_{e}$ and BF_{3} counters and V_{TH}=-0.35V in the ^{235}U counter.

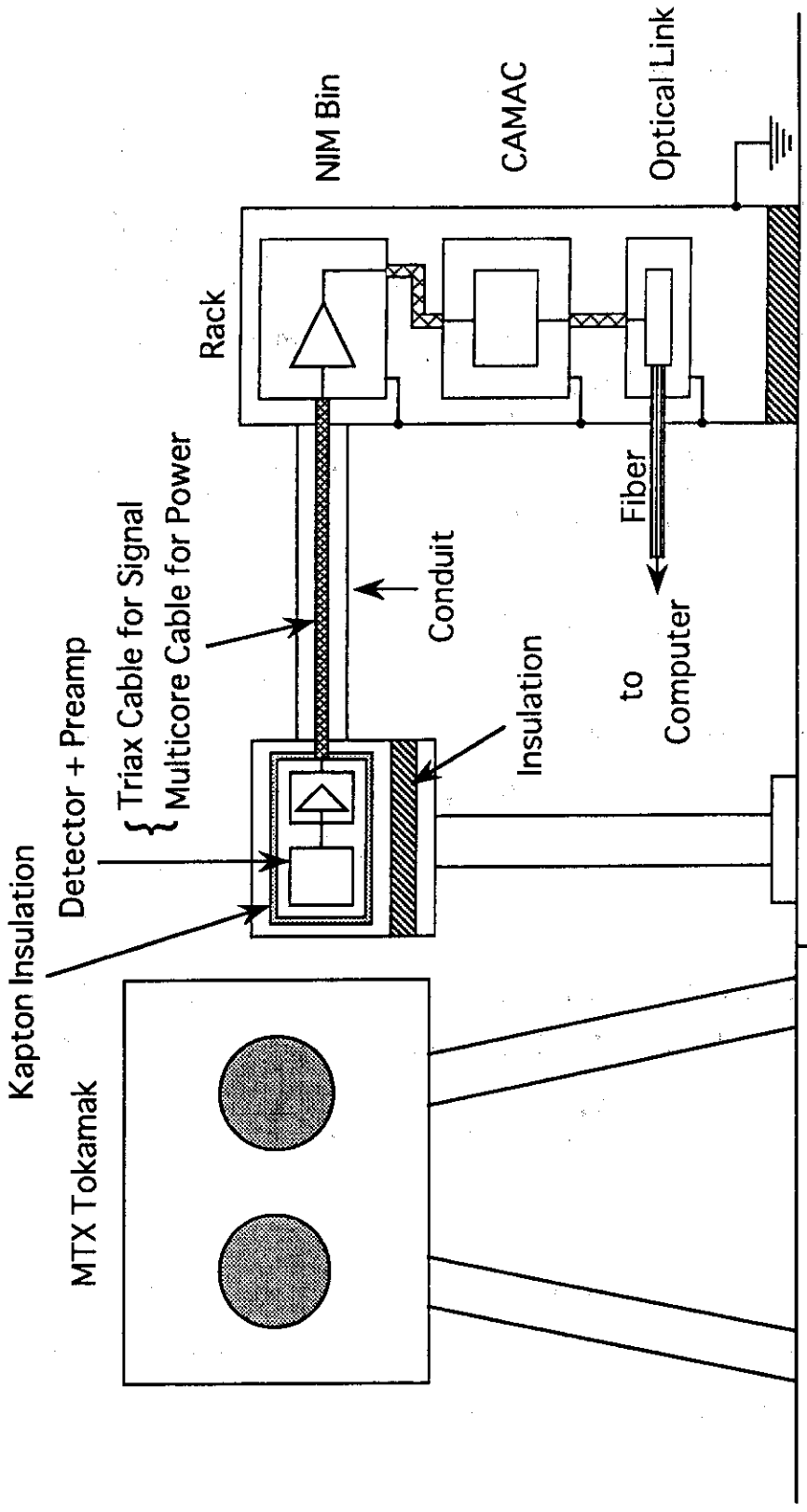

Fig.11 Schematic diagram of the grounding for the neutron diagnostic. All cables between the enclosure and the diagnostic rack are covered with shielding tubes which connect the enclosure to the rack ground.

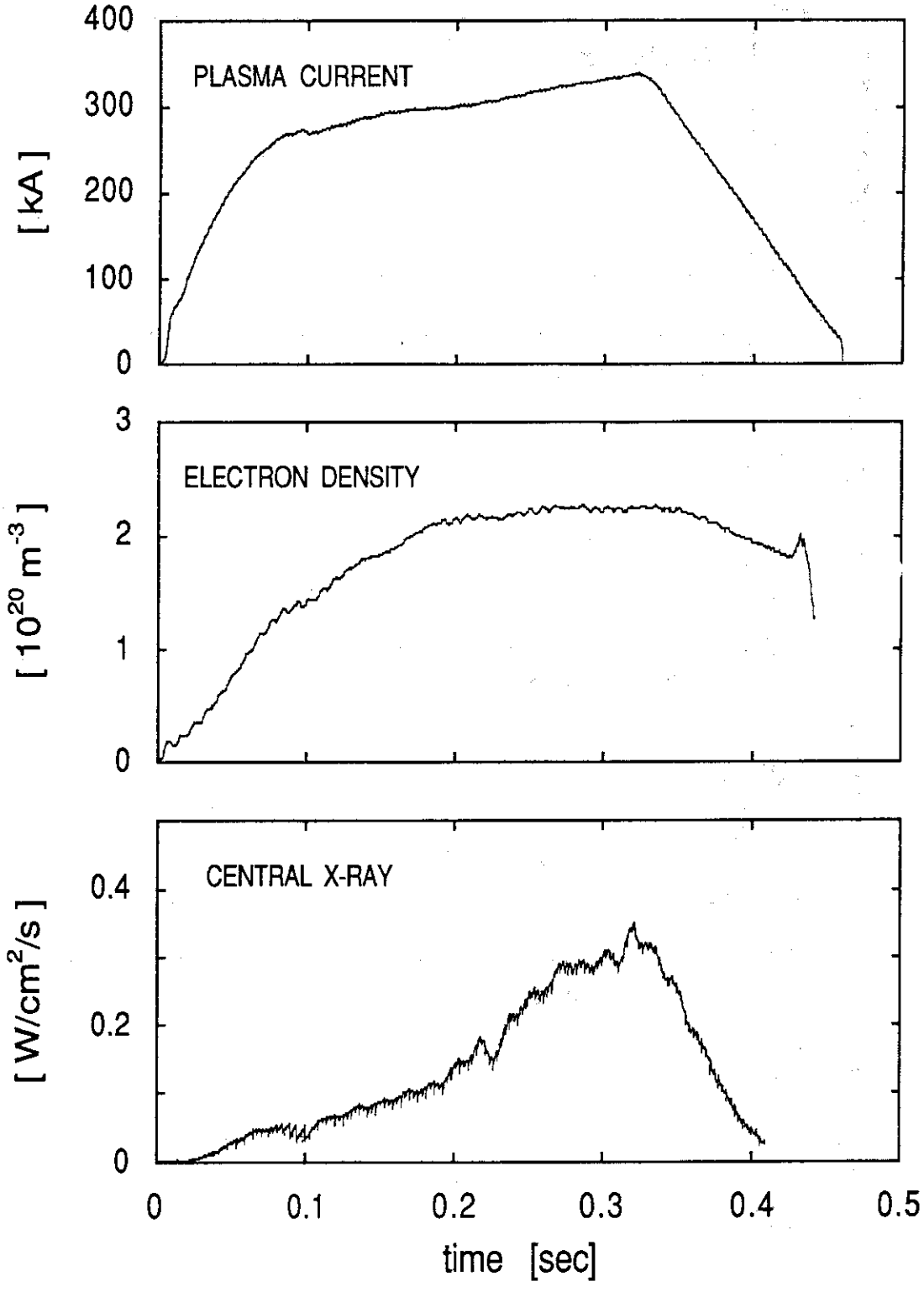

Fig. 12 The time evolution of plasma current, line-averaged electron density and soft x-ray emission for shot No. 8922 on June 7, 1990.

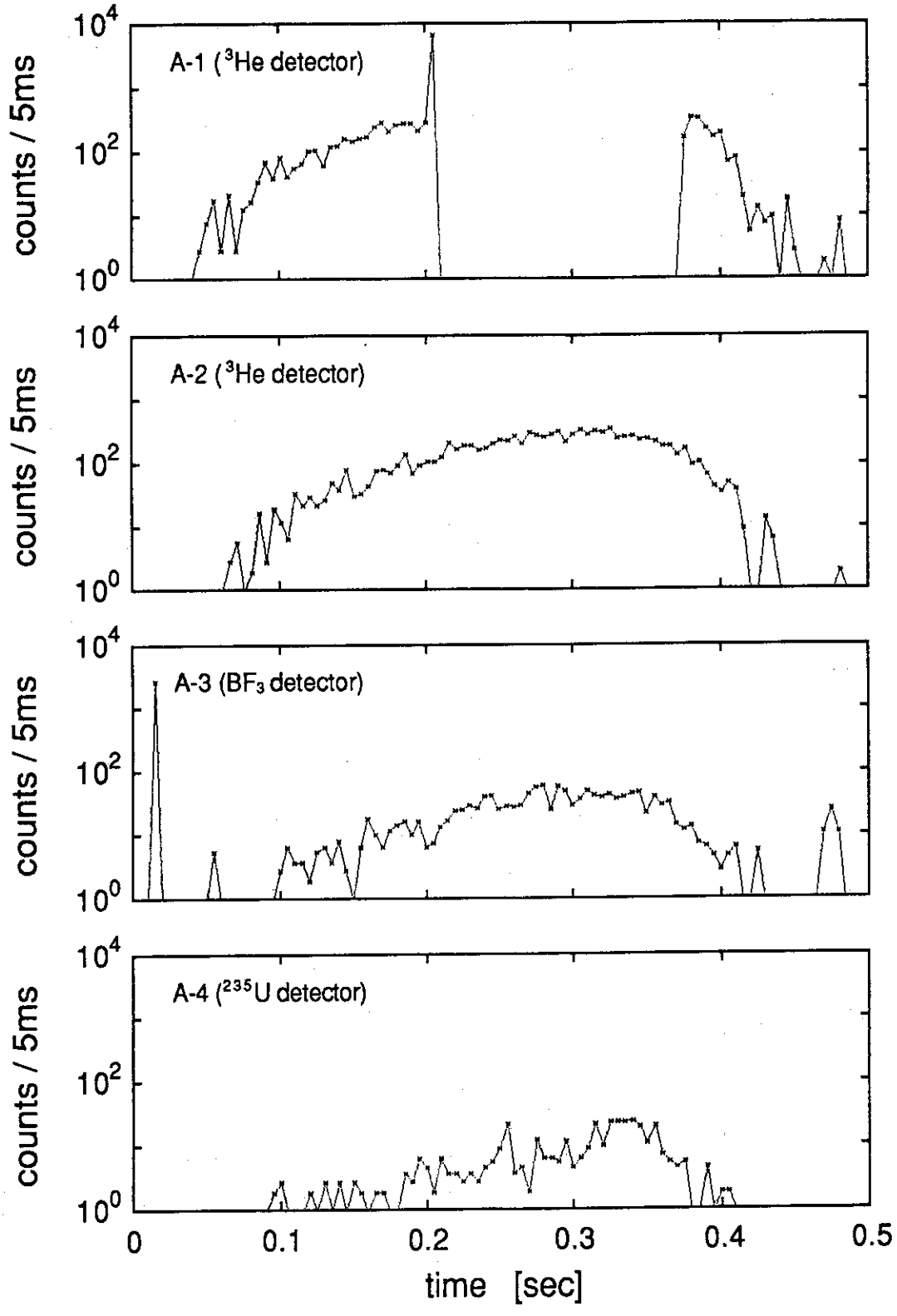

Fig.13 Time evolution of neutron count rates for the same plasma shot as in Fig.12.

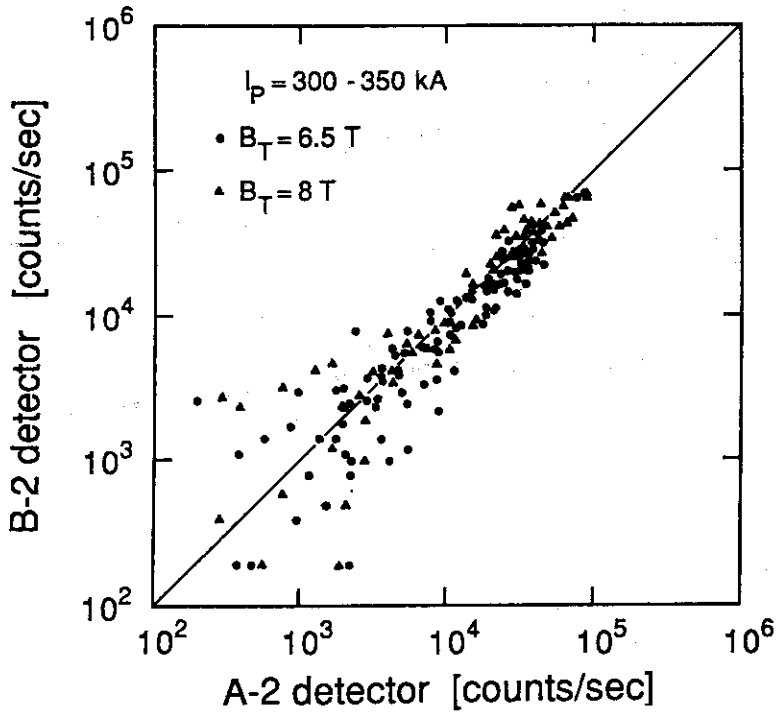

Fig. 14 The comparison of neutron counts at two different toroidal locations, one by a limiter port (B-2 detector) and the other beside a nonlimiter port (A-2 detector).

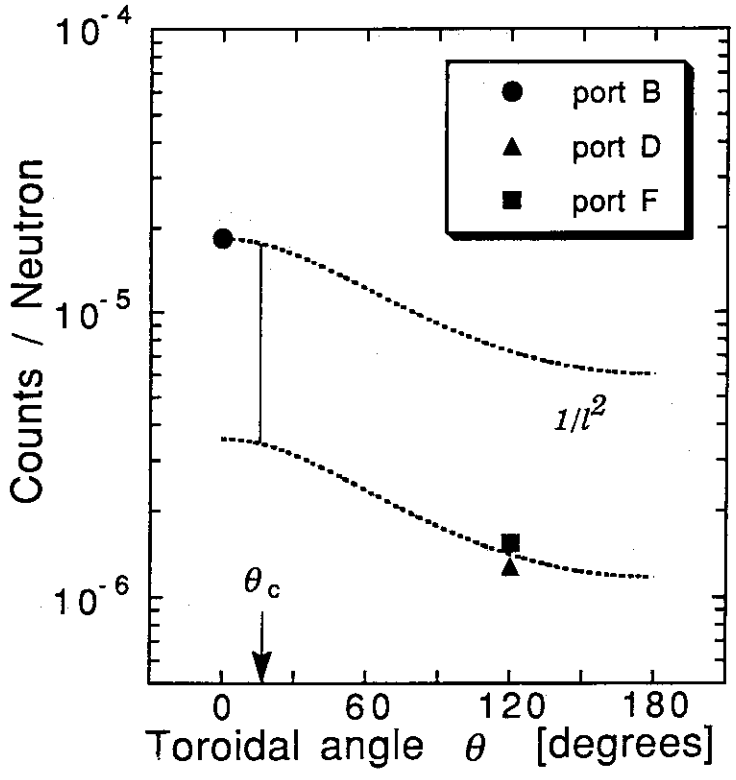

Fig. 15 The detection efficiency of the B-1 detector for the ^{252}Cf source neutrons. The toroidal angle θ is the angle between port B and the source position. The two dotted lines are $1/\ell^2$ curves normalized to the data points at the toroidal angle $\theta = 0°$ and $\theta = 120°$

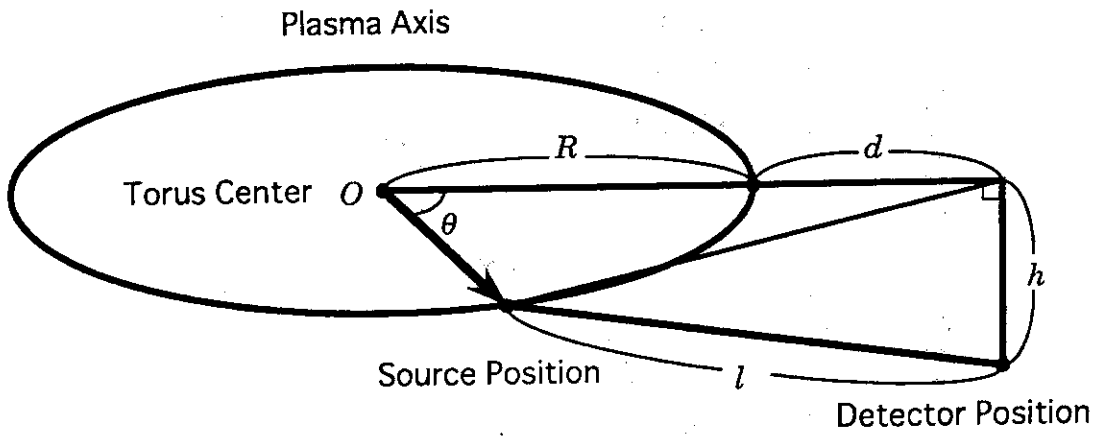

Fig. 16 Schematic diagram of the geometry showing the source position and the detector position.

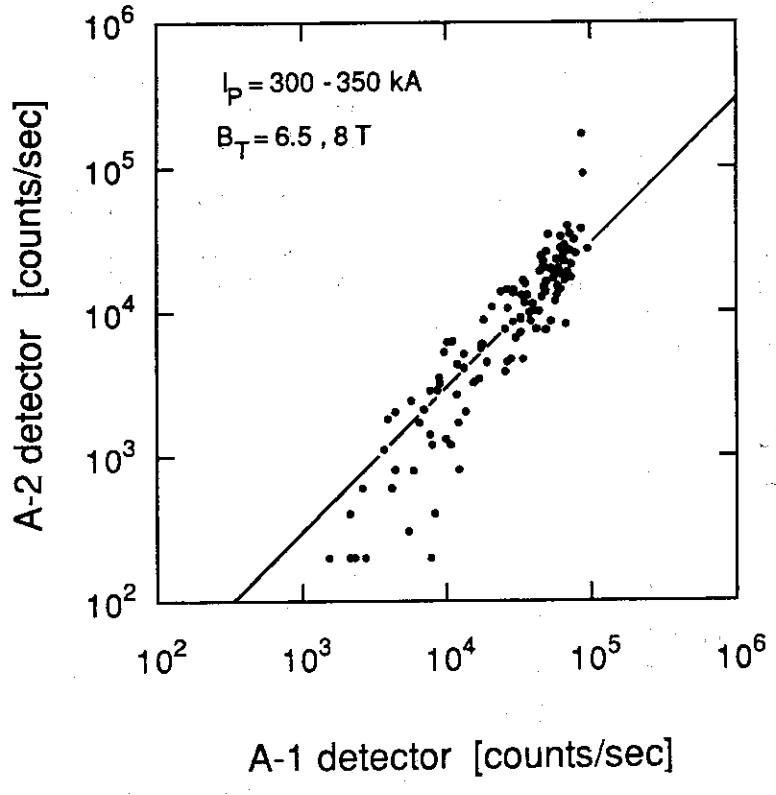

Fig. 17 The relative efficiency of the A-1 detector and the A-2 detector. The plots show detector count rate in standard ohmic plasmas. The straight line shows the relative efficiency obtained from the in situ calibration.

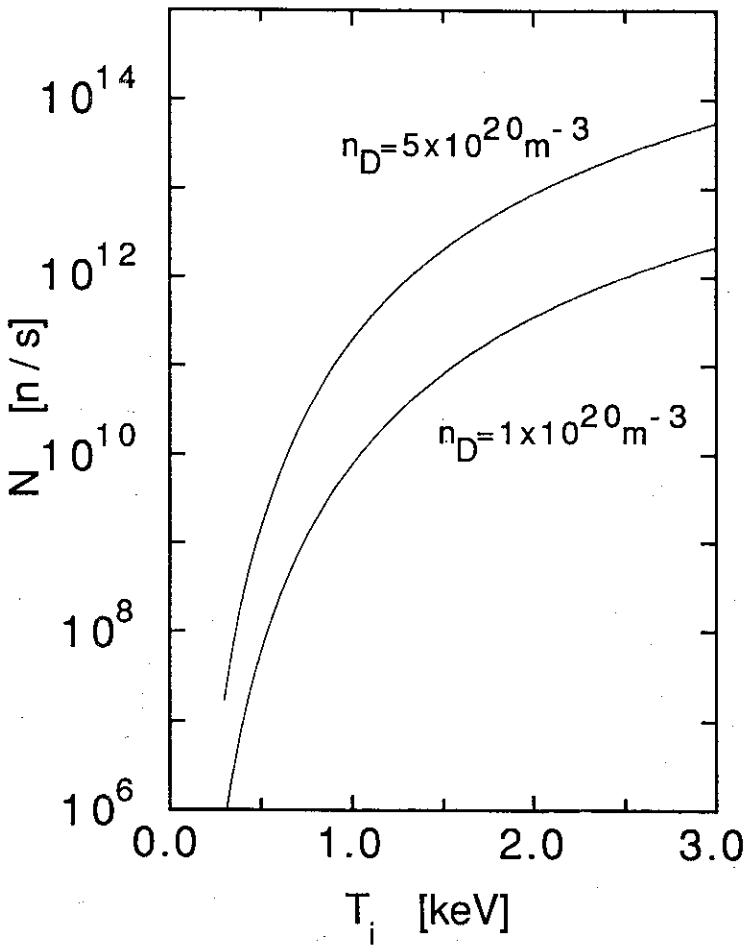

Fig. 18 Calculated neutron production rate versus the central peak ion temperature. Temperature and density profiles of the form $T \propto [1-(r/a)^2]^2$ and $n \propto [1-(r/a)^2]^2$ are assumed. The central deuterium densities are $n_D=1\times10^{20}m^{-3}$ and $n_D=5\times10^{20}m^{-3}$.

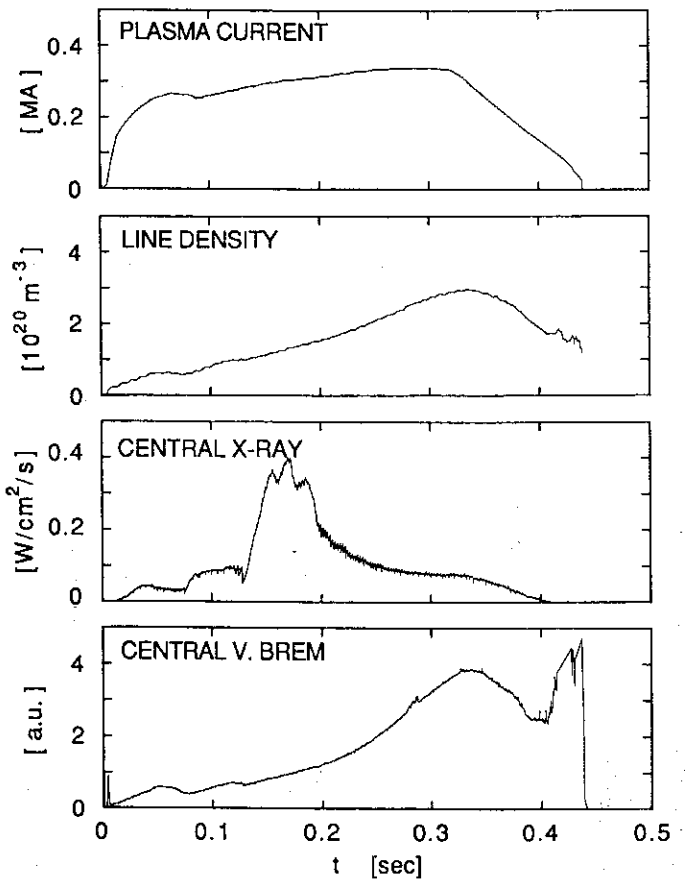

Fig. 19 Time evolution of MTX plasma parameters for the shot No. 7794 on March 28, 1990.

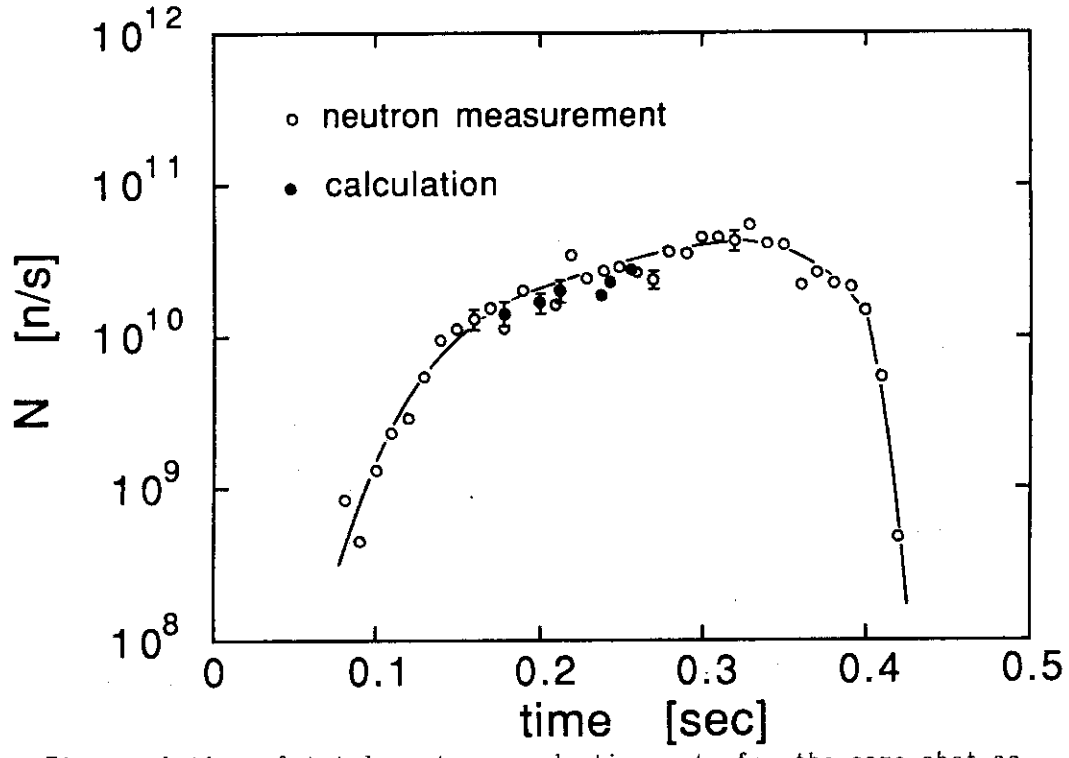

Fig. 20 Time evolution of total neutron production rate for the same shot as in Fig. 19. The open circles show the neutron measurement data and the closed circles show the calculated data from the neoclassical transport study. The calibration factor is calculated for θ_c=15° ± 5° . The uncertainty of the neutron data comes from the calibration factor.

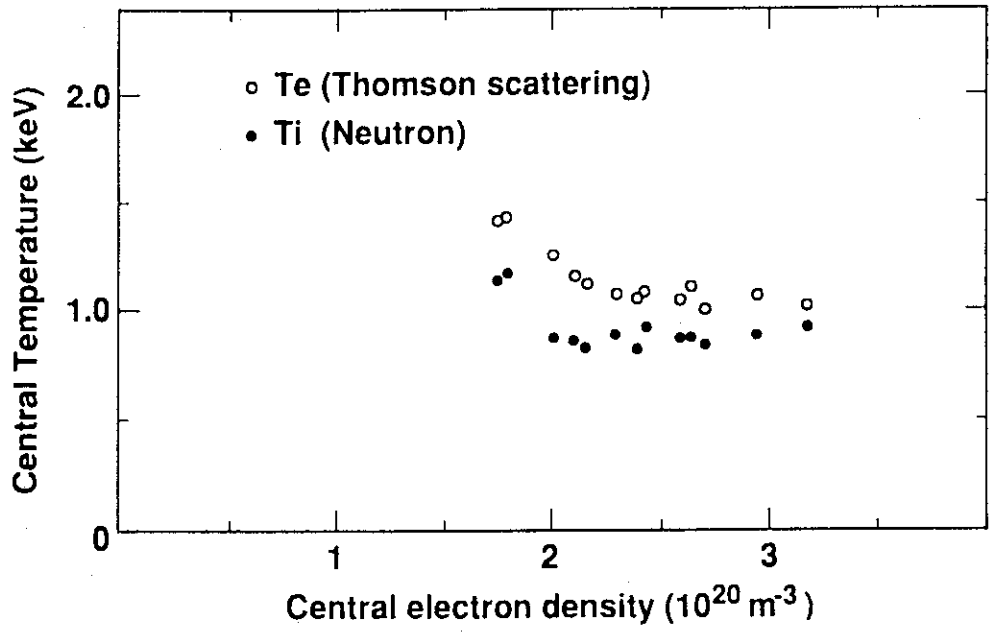

Fig. 21 The ion temperatures deduced from the neutron measurement are shown with the electron temperatures as a function of the central electron density at B_t=8T, I_p=250～400kA.

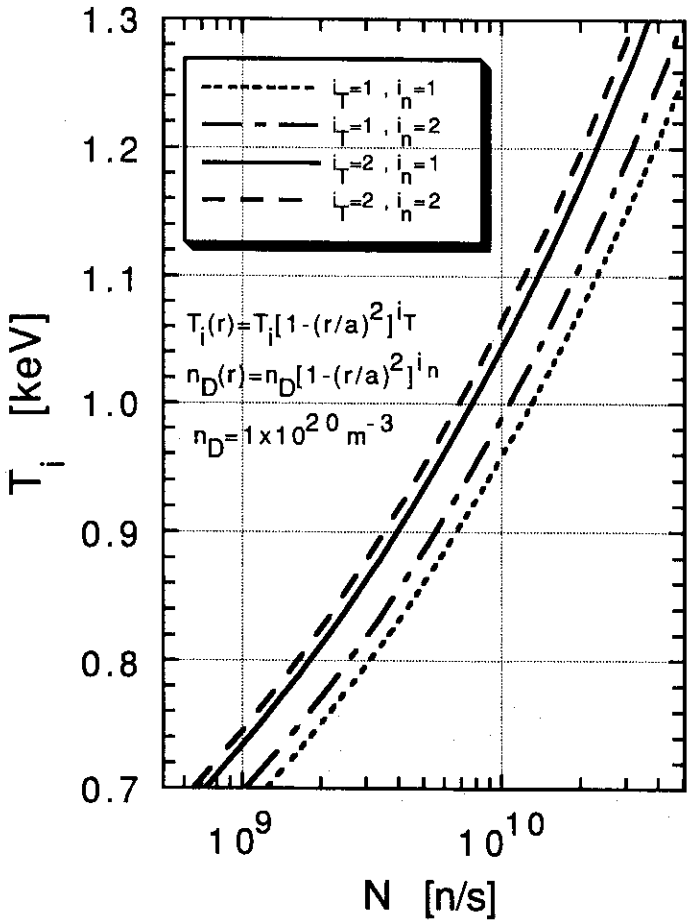

Fig. 22 The central ion temperature calculated from neutron rates showing the dependence on the ion-temperature and deuteron-density profiles.

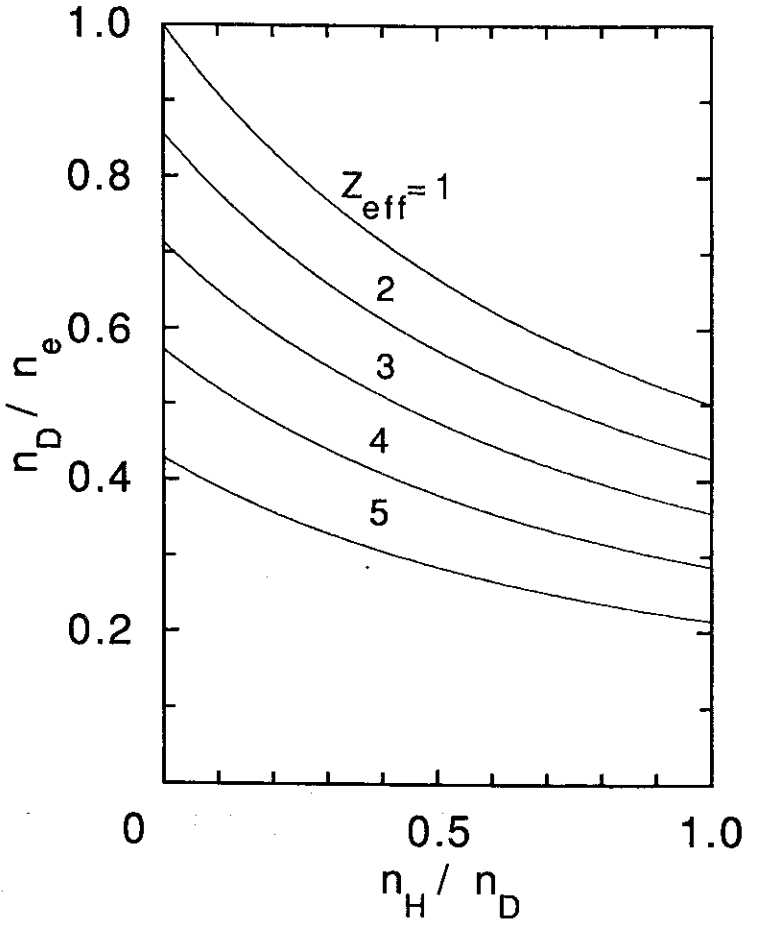

Fig. 23 The ratio of the deuteron to the electron density versus the ratio of the hydrogen to the deuteron density, showing the dependence on Z_{eff}.

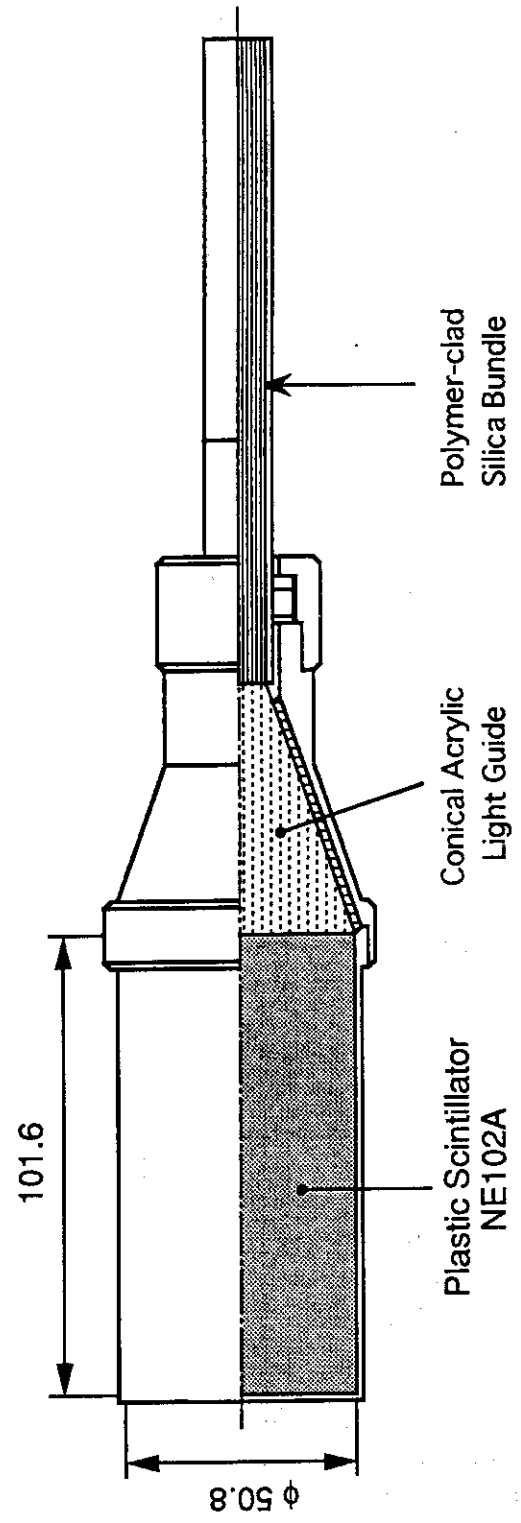

Fig. 24 Schematic diagram of the scintillator system. The scintillator is 5cm in diameter and 10cm in length with a conical acrylic light guide and a polymer-clad silica bundle (20m).

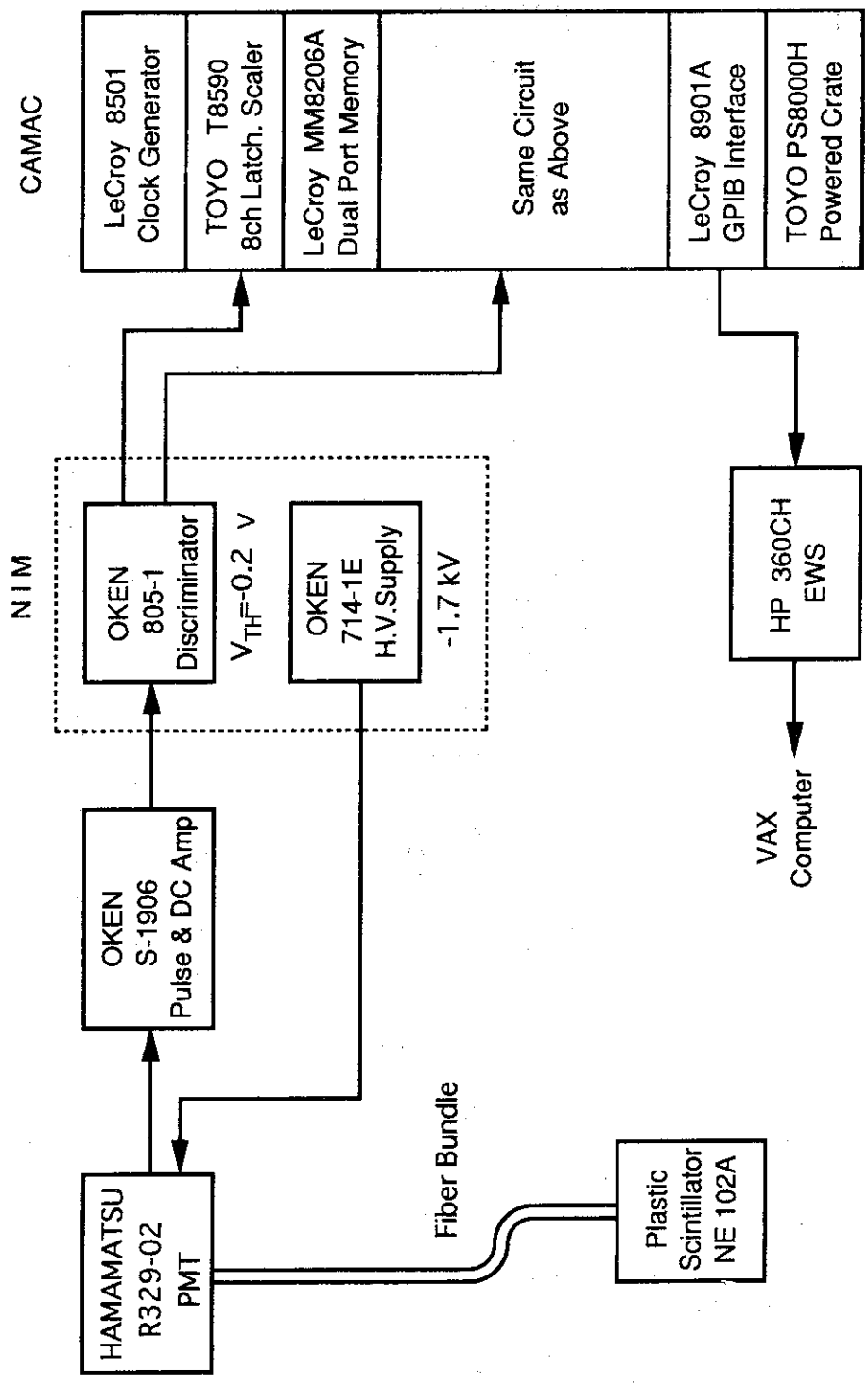

Fig.25 The electronics system for the high-speed neutron measurement. This figure shows only the pulse-count mode operation system. The CAMAC modules are the same as used in the neutron-production-rate measurement system.

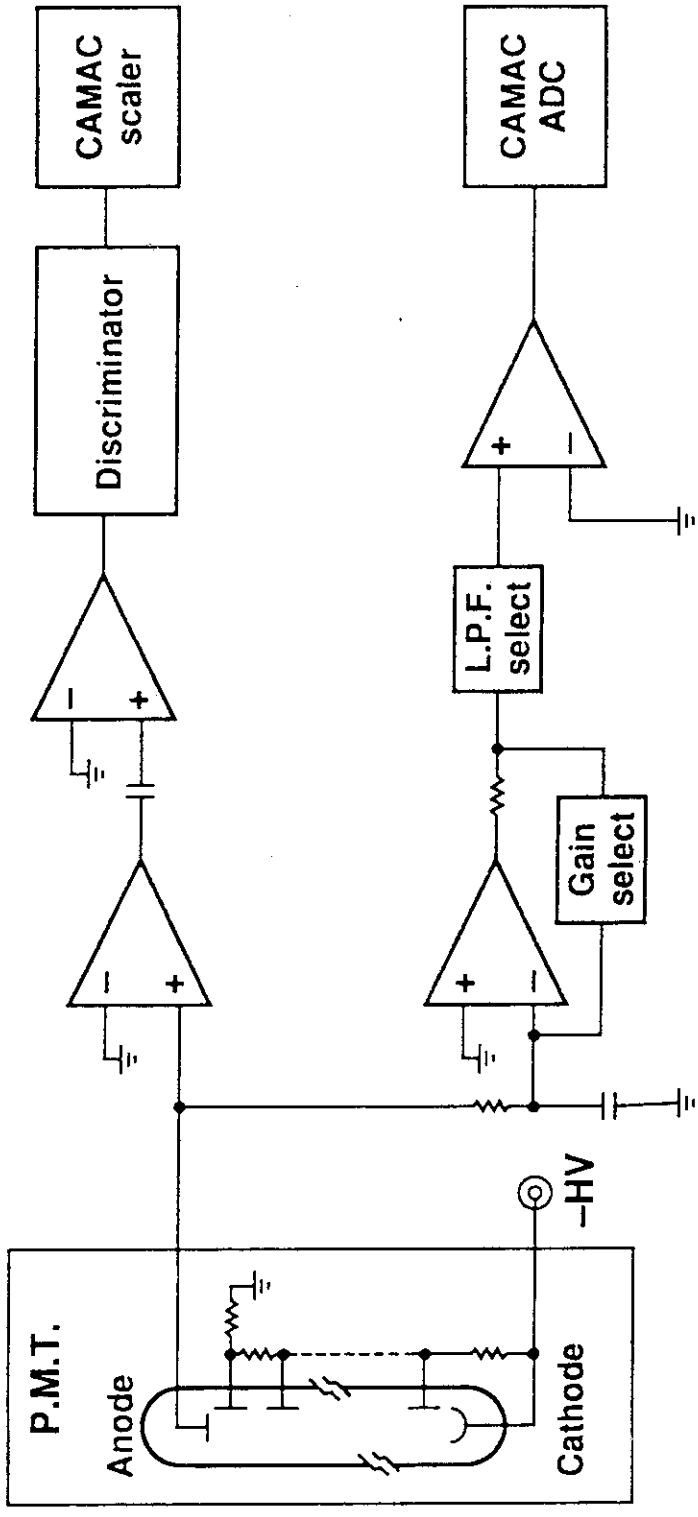

Fig.26 The electronic circuit for the plastic scintillator probe and amplifier. It operates in both pulse-count mode and current mode. The amplifier has fast frequency response, 16MHz in pulse output and 160kHz in direct current output.

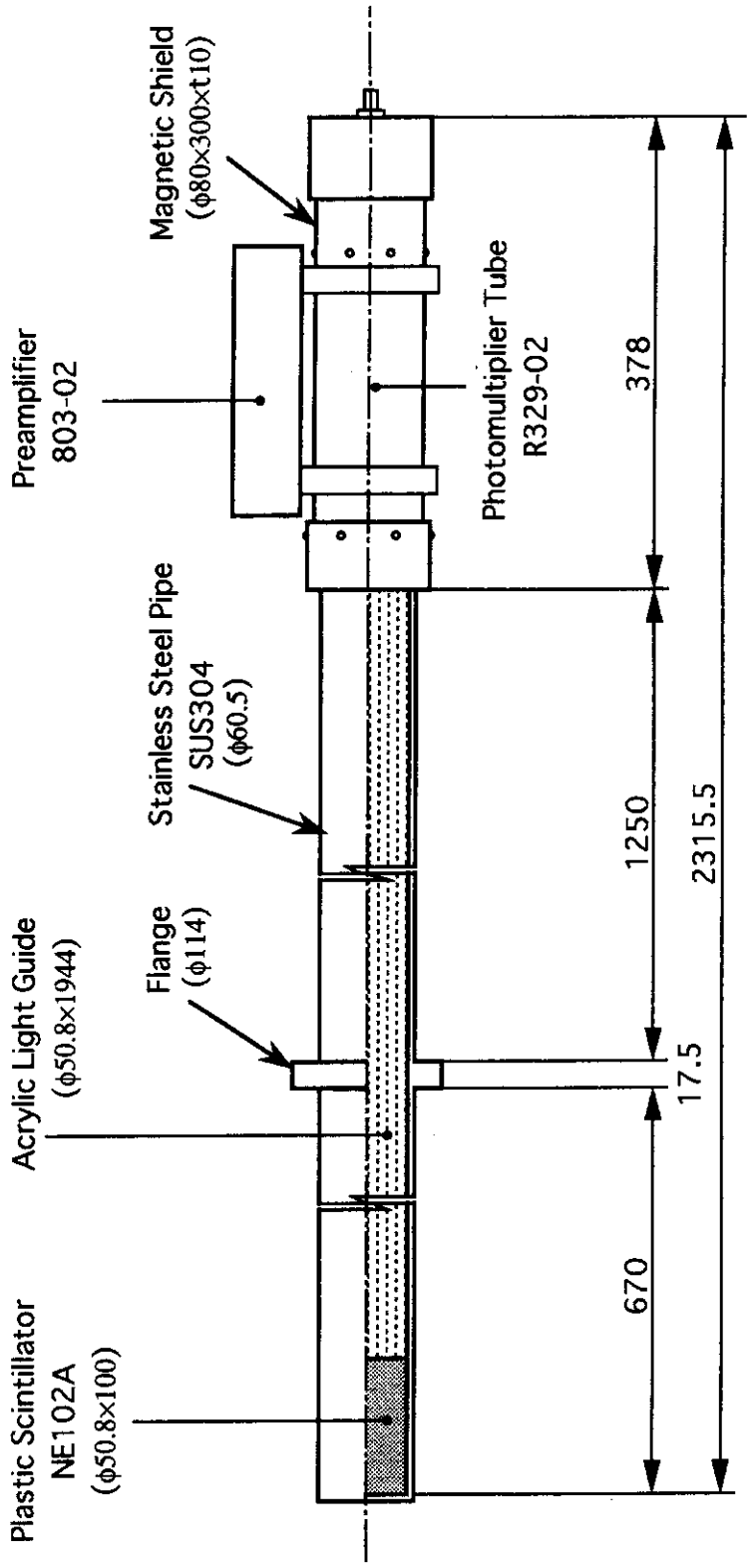

Fig.27 Schematic diagram of the modified scintillator system. A long acrylic light guide is used instead of a fiber bundle to transmit the photon signal to a photomultiplier.

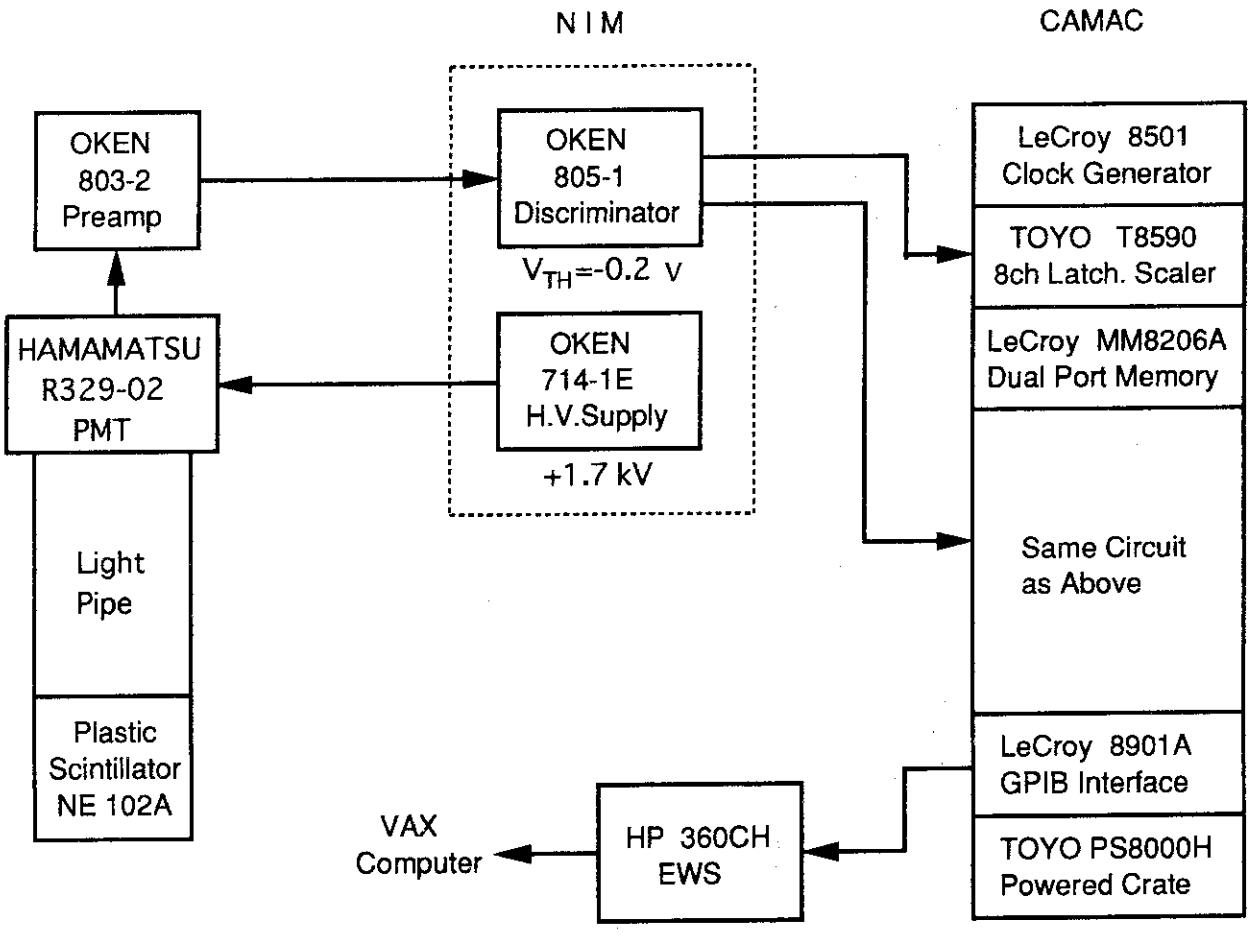

Fig. 28 The electronics system for the modified scintillator system.

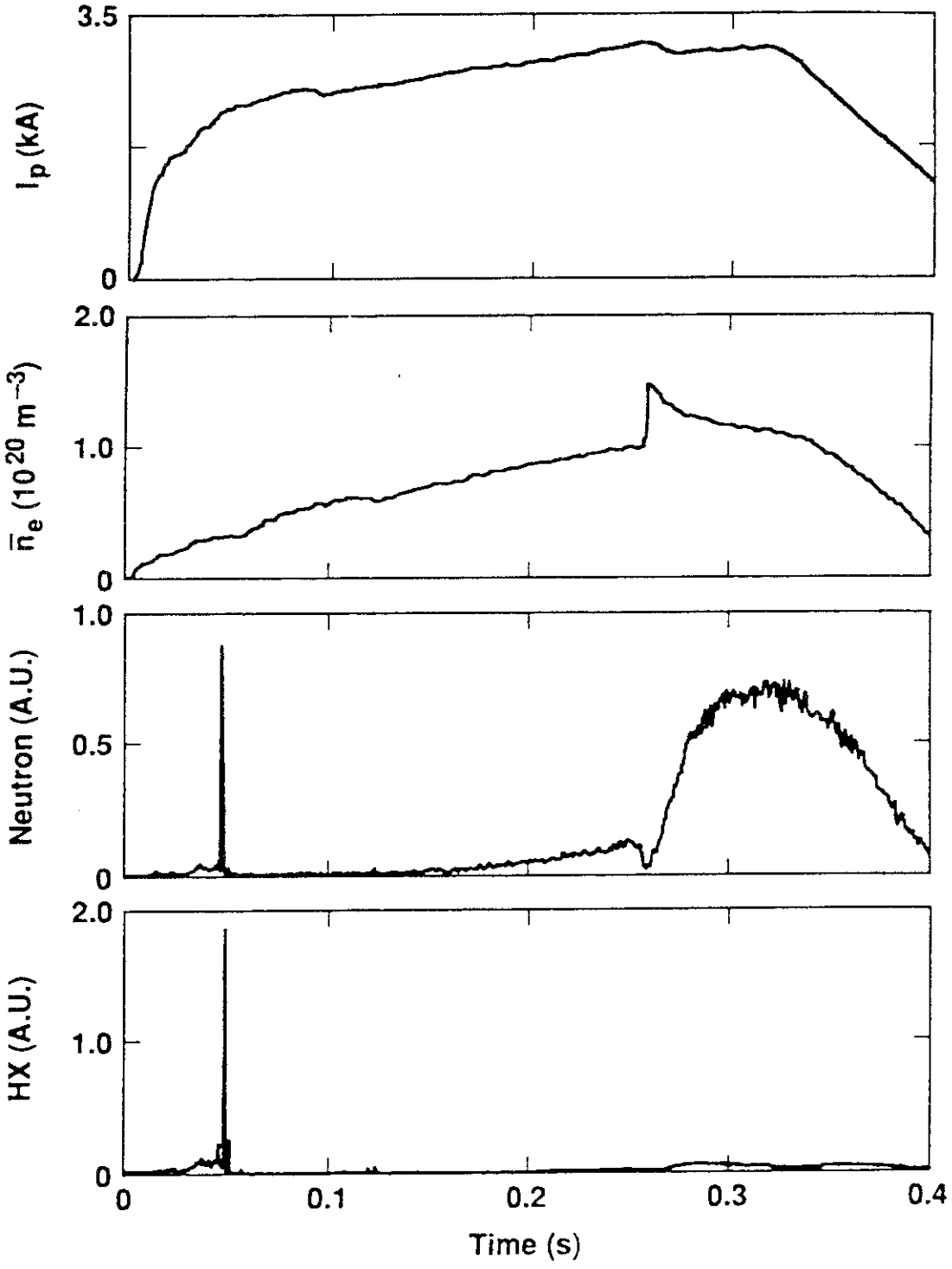

Fig.29 Time evolution of the plasma current, the line-averaged electron density, the neutron signal from the NE102A plastic scintillator, and the hard x-rays in a pellet-injection experiment at B_t=8T. A deuterium pellet is injected into the plasma at 260ms. The sampling time of the plastic scintillator is 1ms in pulse-count mode.